Physics of the Earth and Planetary Interiors 306 (2020) 106500

Contents lists available at ScienceDirect

Physics of the Earth and Planetary Interiors

journal homepage: www.elsevier.com/locate/pepi

A new insight into seismic attenuation characteristics of Northwest Himalaya and its surrounding region: Implications to structural heterogeneities and earthquake hazards

O.P. Mishra, Vandana*, Vikas Kumar, Sasi Kiran Gera

National Centre for Seismology, Ministry of Earth Sciences, New Delhi, India

ARTICLE INFO

Keywords:
Attenuation
P-wave
S-wave
Coda wave
NW Himalaya
Q_α and Q_β
Seismic potential
Earthquake hazards
Seismotectonics

ABSTRACT

The frequency-dependent attenuation characteristics of P-waves (Q_α), S-waves (Q_β) and coda waves (Q_c) in north-west (NW) Himalaya and its surrounding region have been estimated using 515 micro to moderate earthquakes ($2.5 \le M_w \le 5.0$) recorded from January 2008 to November 2015 for a central frequency range (f_c) varying from 1.5 to 12 Hz.

Average attenuation relationships of Q_c, Q_α and Q_β found as: $Q_c = (126.94 \pm 37.9)\cdot f^{(1.122\pm0.06)}$, $Q_\alpha = (65.127 \pm 5.7)\cdot f^{(1.1261\pm0.03)}$ and $Q_\beta = (93.855 \pm 3.05)\cdot f^{(1.1145\pm0.01)}$ for the region. It is found that the nature and extent of seismic attenuation are different for different seismotectonic belts consisted of various kinds of fault systems distributed into the Indo Gangetic Plain (IGP), the Sub Himalaya (SH), the Lesser Himalaya (LH) and the Higher Himalaya (HH) geotectonic segments beneath NW Himalaya and its surrounding region. Material property heterogeneity beneath the subsurface earth is playing an important role in influencing the degree of release of seismic energy in NW Himalaya and its surrounding region because of varying attenuative property in different geotectonic segments [$Q^{-1}\alpha$, β, c(HH) < $Q^{-1}\alpha$, β, c(IGP) < $Q^{-1}\alpha$, β, c(SH) < $Q^{-1}\alpha$, β, c(LH)]. This study may help in better understanding of structural heterogeneities that control the nature and extent of seismogenesis, which in turn may help in assessing seismic hazards through estimates of strong ground motion by computing earthquake source parameters. Our schematic model for NW Himalaya and its surrounding region shed an important light on attenuative characteristics of different tectonic blocks associated with both local and regional fault systems that dictate the source characteristics and potential of earthquake hazards of the region.

1. Introduction

Knowledge of seismic wave attenuation is important as it provides information about the change in the amplitudes and frequency contents of seismic waves with distance from the source. The seismic wave attenuation is primarily needed for making assessments of seismic hazards, strong ground motion, and of earthquake source parameters for different regions (Singh and Gupta, 1979; Singh and Gupta, 1982 Boatwright et al., 1991; Sharma and Wason, 1994; Fletcher, 1995; Chopra et al., 2010; Mishra, 2012; Tripathi et al., 2014; Vandana et al., 2015; Vandana et al., 2016; Kumar et al., 2016; Vandana et al., 2017; Kumar et al., 2019; Vandana and Mishra, 2019; Ekka et al., 2019). Spatio-temporal variation of coda wave (Q_c) has also been studied as an earthquake precursor (Jin and Aki, 1988; Fehler et al., 1988; Vargas et al., 2004; Gholamzadeh et al., 2013). Studying attenuation process helps to infer the physical laws related to the propagation of the elastic energy of an earthquake through the lithosphere. A number of different techniques have been developed to estimate the attenuation characteristics from different types of waveforms recorded on the seismograms. These waveforms include body waves, surface waves and coda waves. The most frequent techniques used to estimate attenuation characteristics at regional distances (<10°) and high frequencies (>1.0 Hz) include: (1) techniques that parameterized the earthquake source and fit a relation in the body-wave spectra (Boatwright, 1978; Hough et al., 1988); (2) methods that cancel the effect of seismic source by taking spectral ratio of different parts of the seismograms (Bath, 1974; Aki, 1980; Frankel et al., 1990); (3) methods that measure the decay of coda amplitude with increasing lapse time (Aki and Chouet, 1975); (4) methods that use a nearby small events as an empirical Green's function (Hough, 1997); and (5) methods that invert the spectra of recorded ground motion to estimate Q and source parameters (Boatwright et al., 1991; Fletcher, 1995). It is pertinent to mention that seismic wave attenuation characteristics have also been estimated using P-waves (Q_α), S-waves (Q_β), coda waves (Q_c), and Lg-waves (Q_{Lg}) recorded at local or regional distances by different researchers for different tectonics, elsewhere in the world (Scherbaum and Kisslinger, 1985; Gupta et al., 1998; Paul et al., 2003; Mak et al., 2004; Sharma et al., 2008; Parvez et al., 2008; Mohamed et al., 2010; Dobrynina Anna, 2011; Singh et al., 2012;

* Corresponding author.
E-mail address: vandana.ghangas@gmail.com (Vandana).

https://doi.org/10.1016/j.pepi.2020.106500
Received 21 February 2020; Received in revised form 13 April 2020; Accepted 22 April 2020
Available online 05 May 2020
0031-9201/ © 2020 Elsevier B.V. All rights reserved.

Boulanouar et al., 2013; Gholamzadeh et al., 2013; Vandana et al., 2015; Vandana et al., 2017; Das et al., 2018; Kumar et al., 2016; Ekka et al., 2019).

Aki (1969) first examined the possibility of using coda waves of local earthquakes to study the lateral properties of heterogeneous earth. Aki (1969) concluded that the coda excitation appears to be independent of epicentre distances <100 km. Aki and Chouet (1975) developed a model to estimate coda Q from the decay of coda waves. This model has been adopted world over to estimate the coda-based quality factor (Q_c). Aki (1980) modified the Aki and Chouet (1975) and Rautian and Khalturin (1978) methods and put forth the coda normalization method. The coda normalization method of Aki (1980) is used to derive frequency-dependent-attenuation-relation for shear waves (Q_β). This method was extended by Yoshimoto et al. (1993) for simultaneous estimates of attenuation from body waves (Q_α and Q_β). This extension allowed estimation of Q_α. It, is however, a series of methodologies has been developed by different researchers to estimate the quality factor (Q) for different regions of different tectonics in the world (Aki and Chouet, 1975; Sato, 1977; Roecker et al., 1982; Pulli, 1984; Wu, 1985; Jin and Aki, 1988; Havskov et al., 1989; Ibanez et al., 1990; Pujades et al., 1991; Canas et al., 1991; Atkinson and Mereu, 1992; Akinci et al., 1994; Latchman et al., 1996).

The objective of the present study is to estimate seismic attenuation characteristics of the medium beneath NW Himalaya and its surrounding region for better understanding the role of structural heterogeneities in association with the seismogenic potential, causing recurrence earthquake hazards in the region. Taking the advantages of large amount of in-house data-set for the region, the present study is directed to deal with the attenuation relationships for Q_c, Q_α, and Q_β for different tectonic zones using single backscattering model (Aki and Chouet, 1975) and extended coda normalization method (Yoshimoto et al., 1993). We also proposed an average attenuation variability model for NW Himalaya and its surrounding region associated with different faults and complex geo-structural features, which in turn may help depict the hidden seismotectonic and its strong bearing on seismogenesis of varying strengths at different depths beneath the region.

2. Geotectonic setup

The Himalaya is one of the most prominent and active intra-continental orogens showing a classical example of topographic relief development in a compressional tectonic regime. The origin of the Himalaya is attributed to the collision of the Indian plate with the Eurasian plate starting about 50 Ma and the persistent convergence that caused a shortening of about 2000–3000 km thereafter (Valdiya, 1998). It has been reported that the ongoing India-Eurasia collision must increasingly be driven by several other forces, including the subduction of the Indian plate further west and east to the Himalaya (Li et al., 2008). From south to north the Himalaya is divided into four major tectonic and physiographic belts namely, the Sub Himalaya (Siwalik), the Lesser Himalaya, the Higher or Great Himalaya and the Tethys Himalaya or Tibet Himalaya (Himadri). The Indus–Tsangpo Suture Zone (ITSZ) is the northern boundary of the Indian plate. The boundary between the Tethys Himalaya and the Great Himalaya is marked by the Trans-Himadri fault. This fault was first identified as the Malari thrust (Valdiya, 1979, 1987), and later redesignated as Trans-Himadri fault (Valdiya, 1987, 1989). The Main Central thrust (MCT) is a major tectonic boundary between the Great Himalaya and the Lesser Himalaya, whereas the Main Boundary thrust (MBT) separates the Lesser Himalaya from the Sub Himalaya (Siwalik). The Himalaya Frontal thrust (HFT) separates the Sub Himalaya from the Indo-Gangetic Plains. Its surface manifestations are visible only at a few places. Many tectonic models have been proposed for the evolution of Himalaya (Seeber et al., 1981; Ni and Barazangi, 1984; Yin and Harrison, 2000) to understand the seismic activity of the Himalayan region. The principal thrusts namely the Main Central Thrust (MCT), the Main Boundary Thrust (MBT), and the Main Frontal Thrust (MFT) support the southward migration of the main deformation front due to its young age and shallow depth. Some restricted segments of these thrusts exhibit neotectonic activity and active faulting on the surface (Nakata, 1989). The major tectonic discontinuity, MCT, divides the two contrasting structures as the Lesser Himalaya and the Higher Himalaya, which possesses contrasting stratigraphy and tectonic features. In northern part of the Lesser Himalaya, the MCT Zone instigate a belt of seismic activity where moderate earthquakes are frequent that are located mostly beneath the Garhwal and the Kumaon Himalaya (Khattri et al., 1989). Arita (1983) recognized another fault named as Munsiari fault or MCT-I characterized by an abrupt change in lithology and metamorphic grade in the MCT shear Zone below the MCT fault. The Lesser Himalayan Crystalline Nappes (LHCN) are formed either due to segments of the MCT hanging wall or thrust sheets carried by imbricates in the MCT footwall (Gansser, 1964). The duplex development in the MCT footwall has been related to the folding of the MCT and the LHCN (Burg et al., 1987) as shown in Fig. 1.

The seismicity in NW Himalaya area (Fig. 1) generally follows the NW-SE trend and the clusters are mainly seen close either to the MCT or to the MBT or in between the MBT and MCT. The study region is found to be associated with a series of moderate to strong earthquakes ($5.0 \le M \le 7.8$) that have caused significant damages to property and loss of lives in past (Vandana and Mishra, 2019).

3. Methodology

(a) Coda waves (Q_c)

We deployed single backscattering model of Aki and Chouet (1975) to estimate Q_c, in this study, which has proven track record of being applied in diverse tectonic Zones discussed recently by Ekka et al. (2019). Based on the single backscattering model, the coda wave amplitude A(f, t) for a narrow bandwidth signal centred at frequency f and at lapse time t, is given as (Aki and Chouet, 1975):

$$A(f,t) = S(f)t^{-\alpha}\exp\left(\frac{-\pi f t}{Q_c}\right) \tag{1}$$

where, S(f) represents the source function at frequency f; α is the geometrical spreading parameter which is taken as '0.5' and '1' for surface waves and body waves, respectively; and Q_c represents the quality factor of coda waves. Eq. (1) can be written as:

$$In(A(f,t),t) = In(S(f)) - \left(\frac{\pi f t}{Q_c}\right) \tag{2}$$

Relation (2) allows estimation of the Q_c from the slope of the straight-line, fitted between ln(A(f,t)) and time 't' based on least-squares iterative process. According to Rautian and Khalturin (1978), the above relations are valid for lapse times greater than twice the S-wave travel time. The frequency dependent relation of Q_c is described by the power law: $Q_c\,(f) = Q_0.\,(f)^\theta$, where "$Q_0$" is the value of Q_c at 1 Hz, and "θ" representing the degree of frequency dependence of Q_c. The logarithm of this equation allows estimation of "θ" and "Q_0" using a simple linear regression. The coda wave at shorter lapse time is primarily attributed to single scattering, whereas with increasing lapse time, the multiple scattering becomes a preferable tool for analysis (Gao et al., 1983). Therefore, this methodology is very much apt for the analysis of our data for NW Himalaya and its surrounding region.

(b) P-waves (Q_α) and S-waves (Q_β)

Estimates of P-wave based quality factor (Q_α) and S-wave based quality factor (Q_β) are made in this study using the method of Yoshimoto et al. (1993). This method is based on the concept of proportionality among the coda spectral amplitude, A_c (f, t_c); the source spectral amplitude of S-waves, S_s (f); and the source spectral amplitude of P-waves, S_p (f), and can be expressed as follows (Yoshimoto et al., 1993):

$$A_C(f,t_c) \propto S_p(f) \propto S_s(f) \tag{3}$$

where, S_p (f) and S_s (f) are the same as defined above, f is the frequency in Hz, and t_c is the reference lapse time measured from the source origin time. Based on the idea of proportionality, the Q_α and Q_β can be calculated from the following expressions by analysing earthquakes occurring at various hypocentral distances.

$$\ln\frac{A_p(f,r)r}{A_c(f,t_c)} = -\frac{\pi f}{Q_\alpha V_p}r + cont(f) \tag{4}$$

$$\ln\frac{A_p(f,r)r}{A_c(f,t_c)} = -\frac{\pi f}{Q_\beta V_S}r + cont(f) \tag{5}$$

Using Eqs. (4) and (5), we can estimate 'Q_α' and 'Q_β' simultaneously. Since the ratio of P to S-wave spectra depends on seismic moment and earthquake

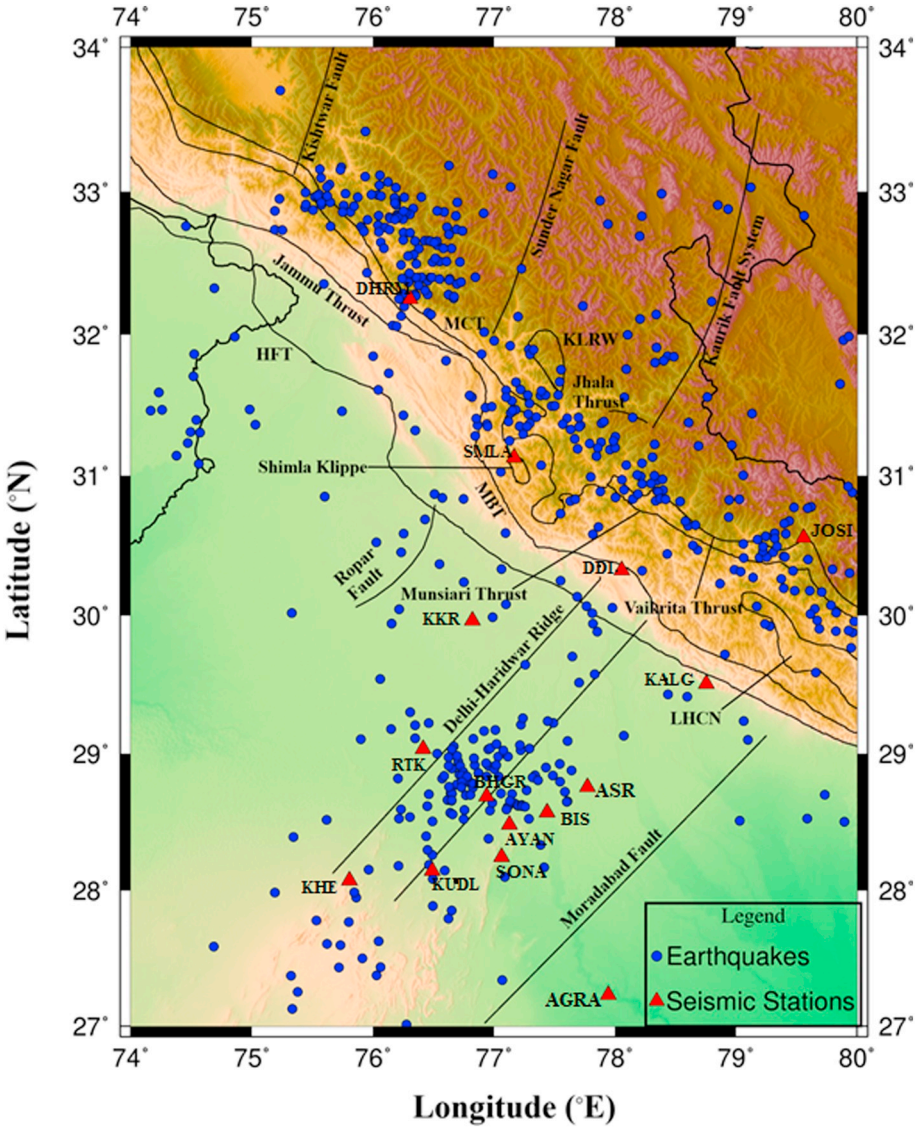

Fig. 1. A map showing tectonic features of NW Himalaya and its surrounding region. Tectonic features in lines are shown as: Main Boundary Thrust (MBT); Main Central Thrust (MCT); Himalayan Frontal Thrust (HFT); Munsiari thrust; Vaikrita thrust; Jammu Thrust (JT); Lesser Himalayan Crystalline Nappe (LHCN), Kullu Larji Rampur Window (KLRW); Jhala thrust. Solid triangles denote seismograph stations in the network and solid circles show the epicentres of earthquakes used in this study. The epicentres of earthquakes are taken from the catalogue by International Seismological Centre (ISC).

magnitude, it is, therefore necessary to restrict the earthquakes of a smaller magnitudes to conduct analysis for estimates of 'Q_α' for the region.

3.1. Data and analysis

Earthquake data set of 515-events of varying magnitude ($2.5 \leq M_w \leq 5.0$) recorded for a period between January 2008 and November 2015 by 15-stations ascribed to the digital seismic network operated by National Centre for Seismology (NCS), Ministry of Earth Sciences (MoES). The epicentres of these 515-events are taken from International Seismological Centre (ISC) bulletin and plotted on the tectonic map of the study area (Fig. 1). We carefully scrutinized the data-set and we used 13-stations to estimate Q_c, Q_α and Q_β. Different stations have different instrument parameterization because of varying sensitivity and precision due to different dynamic ranges of instruments that were deployed for the recording earthquake in the present study. The data recorded with sampling rate of 100 samples per second (sps) were installed at Dehradun (DDI), Dharmshala (DHRM) and Shimla(SMLA) stations with their Nyquist frequency limited to 50 Hz whilst at other stations the data recorded with sampling rate of 50 samples per second (sps) installed at Ayanagar (AYAN), Bahadurgarh (BHGR), Bisrakh (BIS), Joshimath (JOSI), Kalagarh (KALG), Khetri (KHE), Kundal (KUDL), Kurukshetra (KKR), Rohtak (RTK) and Sohna (SONA) with their Nyquist frequency limited to 25 Hz. The waveforms used in this study have high signal to noise ratios (SNR), which is found to be more than three. The digital data recorded by Agra (Agra) and Ausora (ASR) stations were not used in this study because of their low signal to noise ratio. Vertical components of coda-waves were used to estimate Q_c for better clarity since coda analysis found independent of the components of the ground motion analysed (Hoshiba, 1993; Vandana et al., 2015; Vandana et al., 2016; Ekka et al., 2019).

3.2. Analysis of coda waves (Qc)

Records of digital time series of earthquakes in the form of seismograms were selected for the analysis as shown in Fig. 2(a–e) and base line correction was also performed to remove the long period noises and distortions. Selection of three lapse time windows (LTW) of 20, 30 and 40 s were made for estimating Q_c in which Q_c gets computed for particular value at all the stations and at frequencies for all earthquakes. A power law is designed to fit in the form of $Q_c = Q_0 f^{\theta}$, where 'Q_0' is the value of 'Q_c' at 1 Hz and 'θ' is the frequency component. Finally, the estimated power law provides the average coda-Q_c attenuation for the study region.

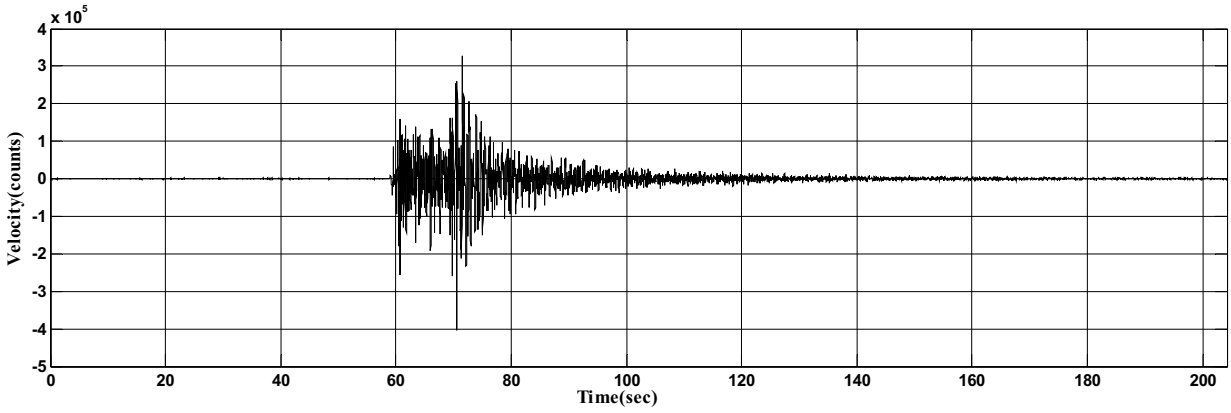

(a)

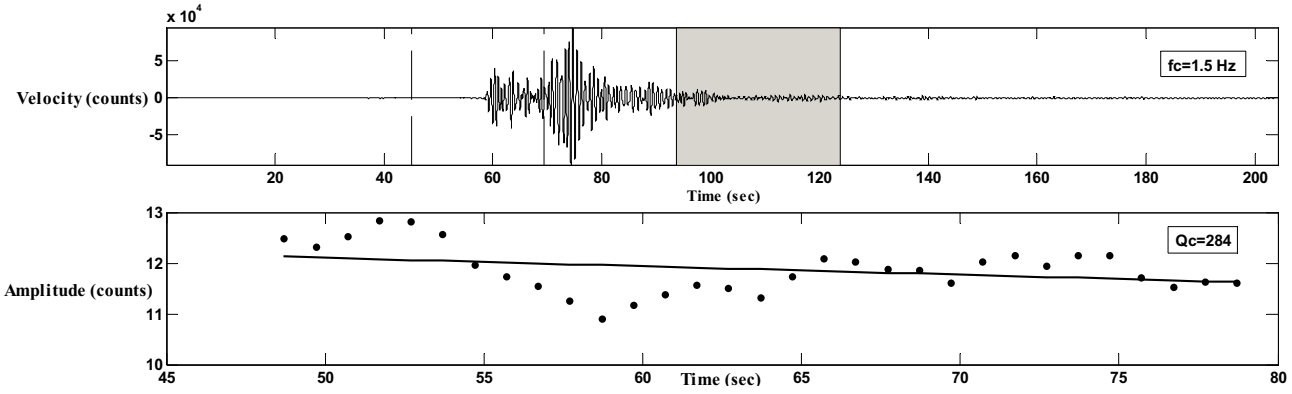

(b)

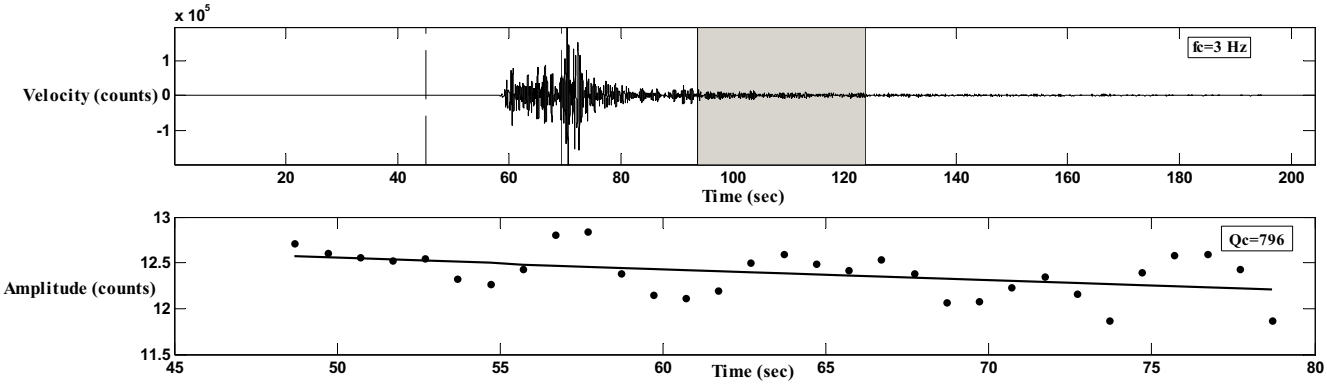

(c)

(caption on next page)

Fig. 2. (a) Plot of unfiltered data trace with coda window of the event recorded by DDI (Dehradun) station on November 27, 2012; (b–e) Band-pass filtered displacement amplitudes of coda window at 1–2 Hz; 2–4 Hz; 6–12 Hz; and 8–16 Hz, respectively, and the RMS amplitude values multiplied with the lapse time along with the best square fit of selected coda window at central frequencies of 1.5 Hz, 3 Hz, 9 Hz, and 12 Hz, respectively. The Q_c is determined from the slope of the best square line; (f) an example of a horizontal-component (north–south) seismogram recorded at station DDI. The arrival time of P (Red colour), S (Pink colour), and coda waves (Green colour) are marked. A time window of 2.56 s is taken for all three waves. (For interpretation of the references to colour in this figure legend, the reader is referred to the web version of this article.)

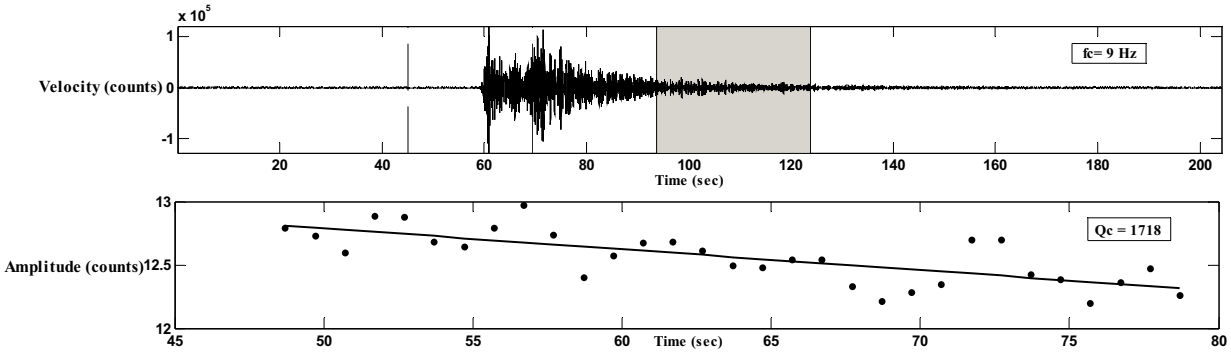

(d)

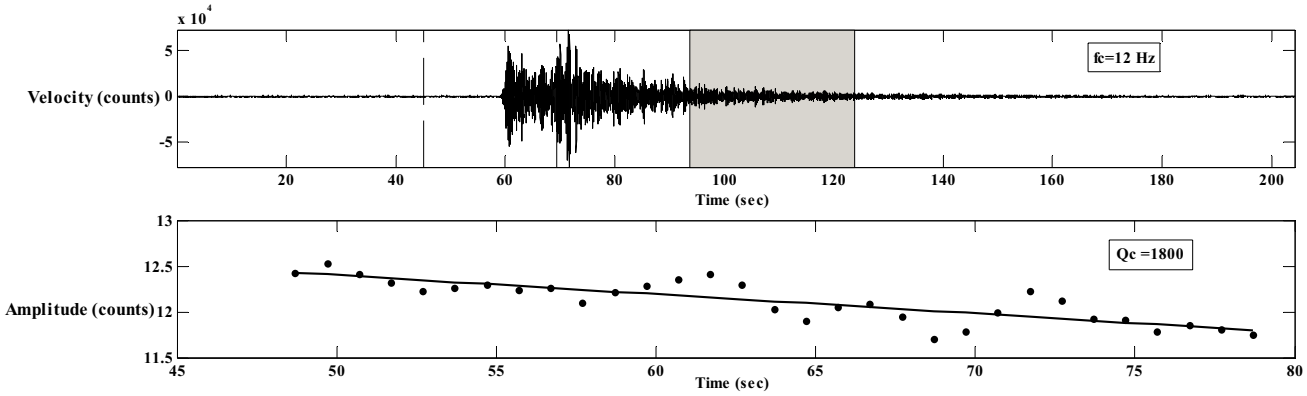

(e)

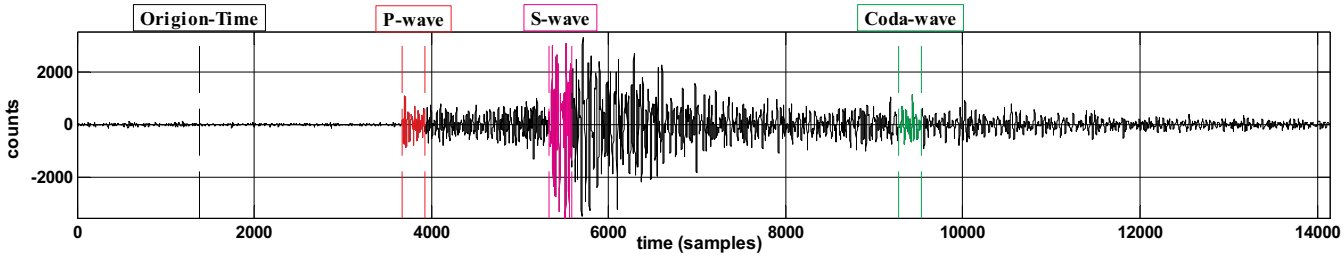

(f)

Fig. 2. (*continued*)

Table 1
Average value of coda quality factor (Q_c) at each station at three different lapse time windows (LTWs) for different central frequencies (f_c) along with Standard error (σ) and number of events (N) used in the present study.

Central frequency (fc)	Lapse time window (LTW)	Station name/Station code (Ayanagar/ AYAN) Qc ± σ	N	Station name/Station code (Bahadurgarh/BHGR) Qc ± σ	N	Station name/Station code (Bisrakh/BIS) Qc ± σ	N	Station name/Station code (Dehradun/DDI) Qc ± σ	N	Station name/Station code (Dhramshala/ DHRM) Qc ± σ	N
1.50	20	164.62 ± 5.94	80	137.21 ± 54.83	191	**92.67 ± 10.42**	174	111.18 ± 11.12	79	127.63 ± 11.24	373
3.00	20	**202 ± 32.92**	80	314.92 ± 48.06	191	**304.50 ± 33.51**	174	**422.52 ± 50.51**	79	280.24 ± 28.08	373
6.00	20	701.86 ± 78.90	80	601.47 ± 75.68	191	**661.21 ± 80.32**	174	728.66 ± 118.42	79	588.96 ± 73.54	373
9.00	20	1195.48 ± 177.84	80	1184.77 ± 113.75	191	1102.54 ± 93.52	174	1476.96 ± 118.60	79	934.87 ± 107.07	373
12.00	20	1621.91 ± 251.17	80	1447.97 ± 158.35	191	1569.12 ± 254.16	174	1648.76 ± 203.26	79	1664.20 ± 173.40	373
1.50	30	178.29 ± 25.78	80	236.03 ± 14.57	191	130.78 ± 19.78	174	168.81 ± 18.55	79	146.26 ± 12.96	373
3.00	30	**223 ± 63.50**	80	409.18 ± 68.90	191	**555.94 ± 60.42**	174	518.23 ± 78.90	79	327.15 ± 33.31	373
6.00	30	963.17 ± 112.49	80	758.48 ± 82.59	191	**986.02 ± 107.21**	174	1196.55 ± 115.94	79	967.81 ± 83.68	373
9.00	30	1567.82 ± 297.55	80	1299.29 ± 117.54	191	2125.36 ± 8.11	174	1886.64 ± 161.43	79	1583.21 ± 100.21	373
12.00	30	2295.93 ± 396.70	80	1749.57 ± 188.35	191	2344.25 ± 716.77	174	2460.79 ± 337.52	79	1773.30 ± 113.68	373
1.50	40	217.55 ± 16.47	80	228.99 ± 28.81	191	203.87 ± 35.80	174	199.21 ± 21.21	79	170.06 ± 16.89	373
3.00	40	387.45 ± 116.99	80	**489 ± 50.38**	191	**478.34 ± 52.52**	174	654.08 ± 98.14	79	383.61 ± 34.08	373
6.00	40	1282.13 ± 133.37	80	1161.72 ± 179.10	191	**1703.17 ± 187.44**	174	1455.38 ± 70.08	79	1147.77 ± 83.12	373
9.00	40	1950.71 ± 258.17	80	1680.62 ± 184.68	191	2898.26 ± 290.71	174	1728.25 ± 154.58	79	1690.14 ± 112.01	373
12.00	40	2572.25 ± 640.00	80	1960.60 ± 160.80	191	2323.12 ± 349.71	174	2433.71 ± 236.49	79	2021.09 ± 142.37	373
1.50	20	118.47 ± 10.48	286	21.64 ± 1.22	183	125.30 ± 17.40	167	138.51 ± 14.48	164	167.22 ± 19.22	181
3.00	20	349.82 ± 31.55	286	261.09 ± 98.75	183	389.42 ± 23.90	167	298.21 ± 61.32	164	342.17 ± 30.42	181
6.00	20	794.76 ± 101.01	286	535.79 ± 156.40	183	1040.48 ± 74.91	167	920.40 ± 193.29	164	894.19 ± 54.66	181
9.00	20	1227.42 ± 116.92	286	834.61 ± 363.24	183	1650.50 ± 87.42	167	1180.38 ± 240.91	164	1337.62 ± 70.08	181
12.00	20	1723.70 ± 193.03	286	990.31 ± 203.62	183	2142.94 ± 154.80	167	1598.88 ± 250.90	164	1936.02 ± 117.74	181
1.50	30	176.13 ± 21.61	286	157.66 ± 76.59	183	182.35 ± 5.55	167	232.25 ± 10.27	164	215.29 ± 29.67	181
3.00	30	400.82 ± 49.93	286	426.18 ± 99.74	183	484.44 ± 39.58	167	381.90 ± 54.73	164	551.81 ± 52.57	181
6.00	30	1098.04 ± 102.83	286	755.12 ± 201.48	183	1546.84 ± 65.08	167	1152.08 ± 105.61	164	1168.22 ± 61.99	181
9.00	30	1493.21 ± 92.03	286	1348.40 ± 361.20	183	1892.65 ± 104.59	167	1616.32 ± 168.17	164	1693.55 ± 68.10	181
12.00	30	1912.06 ± 127.66	286	1753.95 ± 540.20	183	2340.47 ± 199.27	167	1982.91 ± 316.96	164	2015.38 ± 120.11	181
1.50	40	208.17 ± 16.89	286	184.87 ± 48.02	183	230.19 ± 48.16	167	200.95 ± 8.49	164	260.81 ± 22.43	181
3.00	40	486.49 ± 31.27	286	509.56 ± 154.29	183	600.54 ± 66.20	167	615.62 ± 132.36	164	717.57 ± 47.03	181
6.00	40	1117.40 ± 73.34	286	771.23 ± 326.69	183	1513.33 ± 85.74	167	1472.79 ± 123.42	164	1364.86 ± 56.68	181
9.00	40	1563.85 ± 106.31	286	1180.62 ± 303.41	183	2032.25 ± 127.20	167	1408.96 ± 75.15	164	1921.29 ± 84.64	181
12.00	40	2109.69 ± 146.82	286	1460.27 ± 338.87	183	2293.42 ± 105.54	167	2403.43 ± 488.10	164	2310.23 ± 110.06	181

Central frequency (fc)	Lapse time window (LTW)	Station name/Station code (Rohtak/RTK) Qc ± σ	N	Station name/Station code (Shimla/SMLA) Qc ± σ	N	Station name/Station code (Sona/SONA) Qc ± σ	N
1.50	20	154.25 ± 9.91	182	132.19 ± 8.99	356	99.23 ± 12.10	123
3.00	20	**276.70 ± 12.24**	182	366.85 ± 16.21	356	**311.51 ± 34.21**	123
6.00	20	921.02 ± 128.03	182	770.21 ± 53.20	356	1143.01 ± 177.04	123
9.00	20	1340.94 ± 106.46	182	1309.93 ± 67.93	356	1406.98 ± 202.59	123
12.00	20	2127.09 ± 408.97	182	1633.51 ± 86.36	356	1798.25 ± 211.86	123
1.50	30	221.31 ± 20.28	182	174.38 ± 18.04	356	**197.85 ± 21.67**	123
3.00	30	382.22 ± 44.10	182	498.07 ± 20.77	356	**480.43 ± 52.72**	123
6.00	30	910.64 ± 126.63	182	1215.23 ± 54.42	356	1445.04 ± 158.60	123
9.00	30	1628.83 ± 202.34	182	1582.58 ± 75.39	356	1745.31 ± 169.67	123
12.00	30	2504.88 ± 570.57	182	2038.95 ± 108.05	356	2454.07 ± 284.53	123
1.50	40	255.13 ± 6.74	182	245.38 ± 18.45	356	232.69 ± 10.24	123
3.00	40	859.88 ± 128.21	182	637.48 ± 21.25	356	**734.14 ± 81.71**	123
6.00	40	1358.89 ± 155.33	182	1358.80 ± 45.15	356	1491.63 ± 130.43	123
9.00	40	1973.27 ± 302.39	182	1775.47 ± 61.00	356	2109.15 ± 165.97	123
12.00	40	3578.77 ± 1341.36	182	2403.09 ± 115.75	356	3007.99 ± 408.25	123

3.3. Analysis of P-wave (Q_α) and S-wave (Q_β)

In order to understand the nature and extent of crustal heterogeneities we also estimated P-wave attenuation (Q_α) and S-wave attenuation (Q_β) factors from the analysis of vertical components (Z) and horizontal components (north-south) of ground motion respectively. Fig. 2(f) shows a typical example of ground motion recorded at DDI station. The spectral amplitudes of the direct-P and S-waves were measured using 2.56 s time window. Based on study of Aki and Chouet (1975) and Rautian and Khalturin (1978) we calculated lapse time window of 2.56 s, and the lapse time for the analysed portion of the coda wave is taken as twice the travel time of S-waves on spectral amplitude of the coda waves $A_c(f,t_c)$.

In accordance to the time history of earthquakes, the same durations of the P-wave, S-wave and coda-wave were also selected. Further, the window-length was selected to avoid the inclusion of S-waveform in the P-waveform, particularly for events recorded at small epicentral distances, and is given as:

$$\boldsymbol{TimeWindow} = \begin{cases} (\boldsymbol{s}-\boldsymbol{p})s, \; if \; (\boldsymbol{s}-\boldsymbol{p}) < 2.56\,s \\ 2.56\,s, \; if \; (\boldsymbol{s}-\boldsymbol{p}) \geq 2.56\,s \end{cases}$$

The above conditions for choosing lapse time window implies if earthquakes used in this study having epicentre distances lesser than 21 km then the time-window is taken as the exact difference between the arrival time of S-wave and that of P-wave for the used earthquakes whilst for those earthquakes whose epicentre distances >21 km the time-window has been fixed to 2.56 s.

The geometrical spreading is taken as 'r^{-1}' and '$\frac{1}{\sqrt{rh_{moh}}}$' for the epicentral distances $r \leq h_{moh}$ and $r \geq h_{moh}$, respectively (Singh et al., 2012), where 'h_{moh}' is twice the Moho depth (Herrmann and Kijko, 1983; Mahood and Hamzehloo, 2009). In our study region, the estimated average Moho depth is taken as 45 km, in such a way that the deepest Moho may correspond to 90 km as observed beneath western Tibet before shallowing substantially to 50–60 km at the Altyn Tagh Fault (Rai et al., 2006). Hence, our consideration

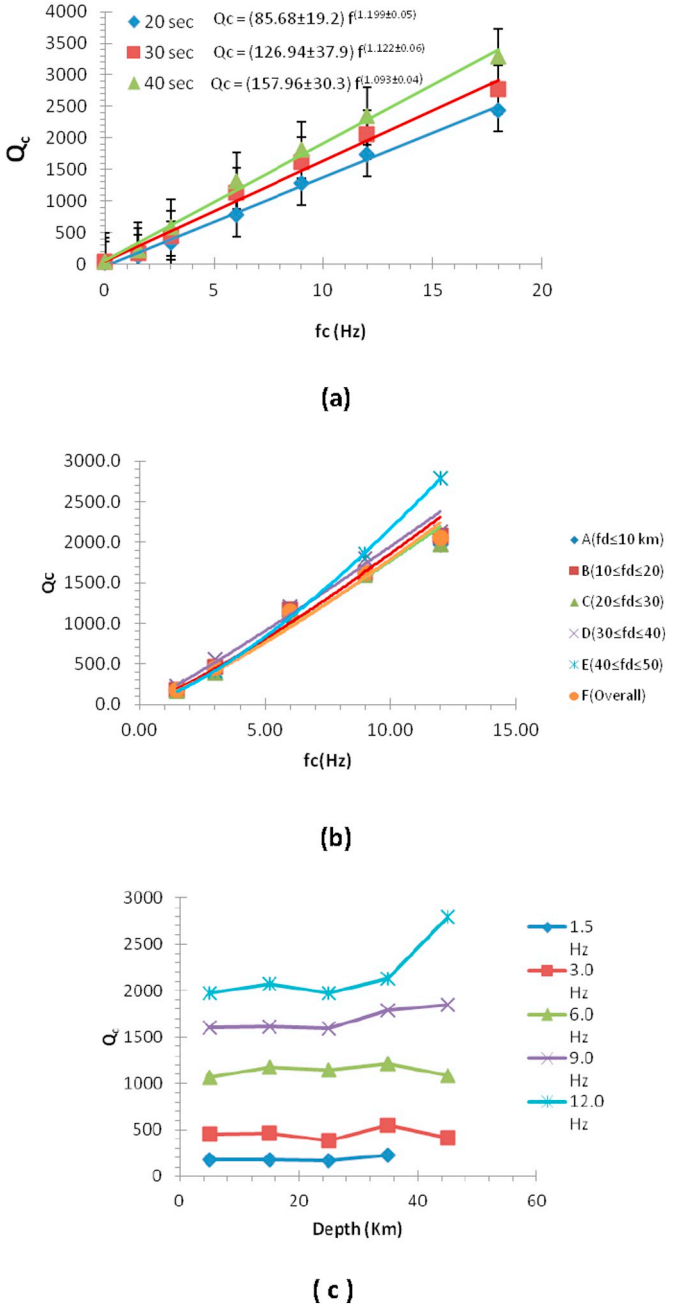

Fig. 3. (a) Plots of average quality factors and central frequencies with linear regression frequency-dependent relationship $Q_c = Q_0 f^{\theta}$ at different lapse time windows (LTWs) of 20 s, 30 s, and 40 s; (b) Plots of average quality factors and central frequencies with linear regression frequency-dependent relationship $Q_c = Q_0 f^{\theta}$ at different depths (f_d) in km, and overall shown in different snap, such as: A for $f_d \leq 10$; B for $10 \leq f_d \leq 20$; C for $20 \leq f_d \leq 30$; D for $30 \leq f_d \leq 40$; E for $40 \leq f_d \leq 50$; and F for Overall; (c) Plots of average quality factors with depth at different central frequencies.

of the Moho depth of 45 km helps to take 'h_{moh}' as 90 km (twice of the Moho depth) in our computation for NW Himalaya and its adjoining region. The hypocenter depths of the earthquakes considered for the analysis was <90 km. Therefore, geometrical spreading has been taken inversely proportional to the epicentre distance (r). Root-mean-square (RMS) spectral amplitudes of the direct P-, S- and coda-wave are computed and the RMS of coda spectrum amplitude used for normalizing RMS spectral amplitudes of P- and S-wave.

The coda based normalized P- and S-wave spectral amplitudes were plotted as a function of hypocentral distance. The slope gives the value of quality factor for P (Q_α) and S wave (Q_β) using Eqs. (4) and (5) at single frequency. Taking averages of all Q values at different stations and at different frequencies, a power law of the form $Q_{\alpha \text{ or } \beta} = Q_0.f^{\theta}$ is fitted for estimating the attenuation relations for both P- and S-wave.

4. Results and discussion

Based on above-mentioned analysis, we obtained an average value of Q_c at each station at three lapse time windows (LTWs) for different frequencies along with the corresponding standard errors as tabulated in Table 1. Our analysis resulted in very intriguing results related to average quality factors of coda waves (Q_c) which has been estimated for various constraints, such as: lapse time, central frequency and depth as shown in Fig. 3(a–c). We also attempted to compare our results with other independent findings made by different researchers for the Himalayan and Peninsular India as shown in Fig. 4(a). Since the tectonics of the present study area for NW Himalayan region is very complex and different researchers have also studied different seismogenic provinces, elsewhere in the world. We also attempted to compare our results with the other tectonic regions, elsewhere in the world studied by different researchers as shown in Fig. 4(b) so that the nature of our estimated crustal heterogeneity can be understood better in sense that which tectonic region of India and out of India corresponds to NW Himalayan region, which in turn may shed an important light on seismogenesis, intricacies of seismotectonic settings and potential of earthquake hazards of NW Himalaya region.

In the present study, we analysed estimated decay of coda-normalized peak amplitudes for P- and S-waves with hypocentral distance at varying central frequencies for DDI (Dehradun) station as shown in Fig. 5(a–j). Attenuation relation for P- wave (Q_α) and S-waves (Q_β) has also been estimated and we compiled their variability at varying frequency as shown in Fig. 6(a). We also compared our results of Q_α and Q_β with the other independent finding of Q_α, Q_β and Q_β/Q_α by different researchers for the Himalayan regions as shown in Fig. 6(b) for Q_α; Fig. 6(c) for Q_β; and Fig. 6d for Q_β/Q_α. Table 2 shows the average values of Q_α and Q_β at different central frequencies at 13-stations. As mentioned above our estimates of both Q_α and Q_β are based on averaging out of all Q values at different stations (N) and at different frequencies, which may have attributed to the smaller error down to 0.001 (Table 2). Table 3(a–c) shows the average attenuation relationships for coda waves (Q_c), P-waves (Q_α) and S-waves (Q_β). We found that average quality factor values at central frequencies varying between 1.5 and 12 Hz in and around various geotectonic segments of NW Himalaya and its surrounding region. We attempted to see the variation of seismic attenuation in different tectonic Zones, such as the zone between Indo-Gangetic-Plain (IGP) and Sub-Himalaya (SH) referred to Zone-1; the Zone between the SH and the Lesser Himalaya (LH) referred to Zone-II; and the Zone between the SH and the Higher Himalaya (HH) referred to as Zone-III with respect to average kappa (κ) (Fig. 7a), with respect to seismic moment (M_0) (Fig. 7b), and with respect to the number of events used (Fig. 7c) in these seismotectonic Zones. Finally, we deduced attenuation based tectonic model for better understanding of the attenuative characteristics of the region (Fig. 8a–b). Table 3a shows the average attenuation relationships for Q_c, Q_α and Q_β estimated for various geotectonic segments of NW Himalaya and its vicinity. Table 3(b–c) shows the average quality factor and average attenuation values at different frequencies varying between 1.5 and 12 Hz for different geotectonic segments to understand the intrinsic attenuation characteristics of the materials underneath these blocks. Table 4 shows the distribution of attenuation parameters (Q_c, Q_α and Q_β), kappa (κ) and seismic moment along with the distribution of number (N) of earthquakes ($M > 4.0$) in different tectonic blocks. We attempted to see the variability of Q_c, Q_α and Q_β in NW Himalaya and its surrounding region to understand why and how these variability of seismic attenuation characteristics of the region are associated with the nature and extent of structural heterogeneities and seismogenesis, which in turn can shed light on the degree of earthquake hazards of the region.

As mentioned above, the single backscattering model is used to analyse the seismograms recorded by 13-station network at three lapse time windows (LTWs) for 20, 30, and 40 s for given central frequency. The average estimates of Q_c are shown in Table 1, which demonstrates that for a given central frequency Q_c found increased for increasing value of LTWs. It is also observed that for a given LTWs, Q_c attains higher values for increasing central frequency (Table 1). Thus, the Q_c increases with an increase of frequency as well as LTW. A power law, $Q_c = Q_0 \cdot f^{\theta}$, is fitted to the data for different LTWs (Fig. 3). The average attenuation relationships are $Q_c = (85.68 \pm 19.2) \cdot f^{(1.199 \pm 0.05)}$,

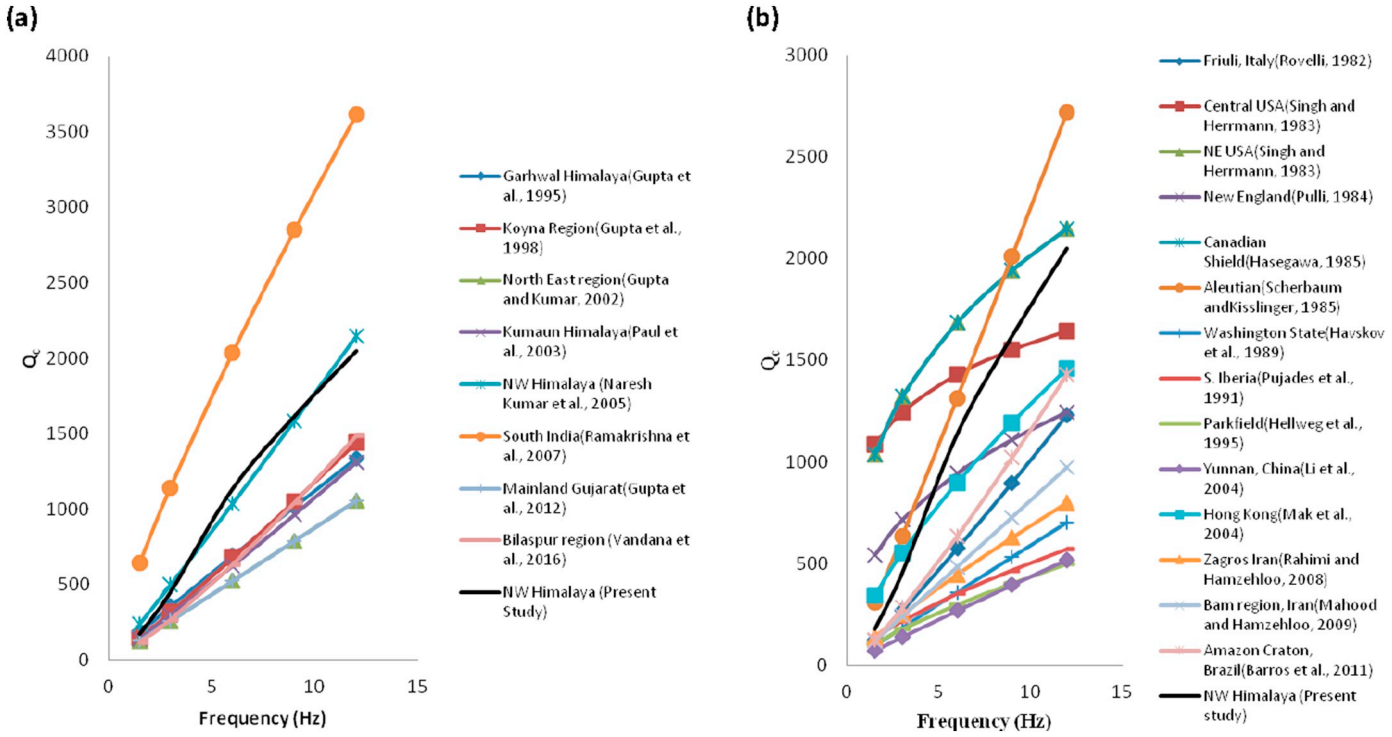

Fig. 4. Comparison of Q_c estimates for NW Himalaya region with (a) other Himalayan and peninsular Indian regions and (b) with other parts of the world.

$Q_c = (126.94 \pm 37.9)\cdot f^{(1.122\pm0.06)}$ and $Q_c = (157.96 \pm 30.3)\cdot f^{(1.093\pm0.04)}$ for LTWs of 20, 30 and 40 s, respectively. It is found that 'Q_0' ('Q_c' at 1 Hz) increases as the lapse time increases, and the 'θ' value decreases with the lapse time windows. The increase in Q_c and decrease in the 'θ' value show a depth dependent character at larger time window that may reflect the effect of deeper part of the Earth. Hence, the increase of 'Q_c' and decrease of 'θ' may be attributed to the increase in depth as heterogeneity decreases with depth by enhancing homogeneity due to compaction, which are in good unison to earlier seismological results obtained independently by different researchers using different methods for estimating different crustal attributes related to its strength and heterogeneities (Sharma and Wason, 1994; Zhao et al., 2002; Mishra et al., 2003; Mishra and Zhao, 2003; Zhao et al., 2004;Mishra et al., 2011; Lei et al., 2012; Mishra, 2013; Mishra et al., 2014; Mukhopadhyay and Tyagi, 2007; Tripathi et al., 2014; Vandana et al., 2017). Woodgold (1994) tried to explain the increase in Q_c with lapse time in sense that the variation in Q_c might have occurred due to non-zero source receiver distance with anisotropic scattering associated with single scattering. Hence, the variation of Q_c with lapse time is because of the variation of attenuation with depth, and it indicates that the medium homogeneity increases with depth. Fig. 2b shows average quality factors and central frequencies at different depths A [$f_d \leq 10$ km]; B[$10 \leq f_d \leq 20$]; C[$20 \leq f_d \leq 30$]; D[$30 \leq f_d \leq 40$]; E [$40 \leq f_d \leq 50$], and F [Overall]. This observation demonstrates that at depth of 40–50 km the increase of frequency corresponds to increase of Q_c value. It is worth to mention that larger lapse times correspond to larger depth (Pulli, 1984). Hence, increase in the Q_c with lapse time window implies the increase of Q_c with depth. Fig. 3c shows average quality factors with depth at different central frequencies since the shallower crust is generally associated with lower strength for shallow focus events with low stress drops (Sharma and Wason, 1994), which suggests that at higher central frequencies, quality factor (Q_c) increases and is very much corroborative with the higher Q_c value at higher frequency range. However, beyond 36 km depth there is a sharp rise in Q_c value, which may be due to structural control or rheological characteristics of the rocks beneath the study region. It is so because increase of depth increases rock compaction due to higher lithostatic pressure on deeper depths that supports the interpretation based on 3-D velocity tomographic results for regions elsewhere in the world (Zhao et al., 2004; Li et al., 2008; Mishra et al., 2008; Lei and Zhao, 2016).

Fig. 4a, shows a comparison of Q_c estimates of NW Himalaya with the other Himalayan and peninsular Indian regions. We obtained frequency dependent attenuation relation as: $Q_c = (126.94 \pm 37.9)f^{(1.122\pm0.06)}$ at 30 s LTW. It is found that the average variation of Q_c in the study region is close to the model of NW Himalaya obtained by Kumar et al. (2005), which depict similarity in the regional geology in NW Himalaya and its surrounding region (Kumar et al., 2005). Fig. 4(b) shows a comparative study of the Q_c estimates in the present study with some of the global studies made by different researchers for different regions using different data set (Li et al., 2004; Havskov et al., 1989; Hellweg et al., 1995; Rovelli, 1982a, 1982b; Mak et al., 2004; Mahood and Hamzehloo, 2009; Rahimi and Hamzehloo, 2008; Pujades et al., 1991; Barros et al., 2011) to ascertain what tectonic settings of NW Himalaya corresponds to other tectonic blocks, elsewhere in the world. We found that our assimilated model is comparable to that of the Aleutian region (Scherbaum and Kisslinger, 1985), signifying the fact that both these regions are seismically very active and exist in the underthrusting tectonic regime.

The Quality factors, Q_α and Q_β, are determined at six central frequencies for NW Himalaya and its surrounding region. The variations in quality factor at all the 13-stations are listed in Table 4 is observed that Q_α and Q_β increases with the frequency. A power law, $Q_c = Q_0.f^\theta$ (in which Q_0 is the Q value at 1 Hz and θ is the frequency exponent) is fitted for each station from the Q_α and Q_β values.

We obtained the average Q_α and Q_β relations as: $Q_\alpha = (65.127 \pm 5.7)\cdot f^{(1.1261\pm0.03)}$ for the P-wave; and $Q_\beta = (93.855 \pm 3.05)\cdot f^{(1.1145\pm0.01)}$ for the S-wave as shown in Fig. 5a. The frequency-dependent Q_α and Q_β relations are compared with those obtained in other seismically active regions of the Himalaya (Fig. 6b–c). These include the Garhwal region in the Western Himalaya (Sharma et al., 2006; Sharma et al., 2007; Negi et al., 2014; Sharma et al., 2009; Tripathi et al., 2014), the Kumaon region in the Northwestern Himalaya (Imtiyaz et al., 2012; Singh et al., 2012), the Sikkim region in the Eastern Himalaya (Hazarika et al., 2013), the Kinnaur and Bilaspur regions of the Himachal Himalaya (Kumar et al., 2014; Vandana et al., 2016). It is found that our estimates of Q_α made in the present study (Fig. 6b) are much more comparable with that of the Bilaspur region of the Himachal Himalaya (Vandana et al., 2016). It is interesting to note that our estimate of Q_β for NW Himalayan region is not comparable with that of the Bilaspur region of the Himachal Himalaya by Vandana et al. (2016). Our estimate of Q_β (Fig. 6c) is almost comparable to that of Imtiyaz et al. (2012), which were made for NW Himalayan region. The primary reason of such variability is attributed to the distinct geology of the region where it is principally associated with the metasedimentary, sedimentary, igneous and metamorphic types of rocks, which

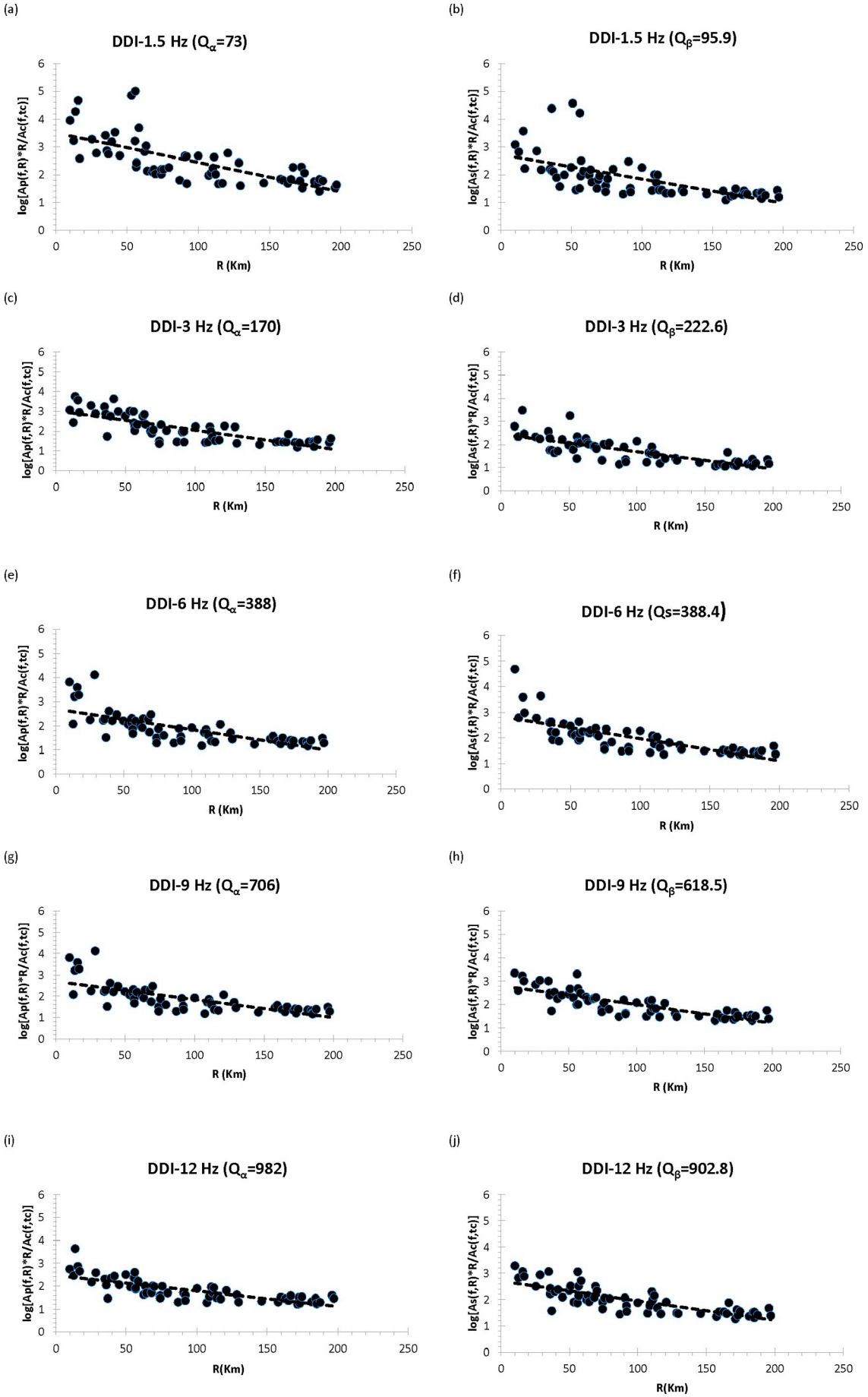

Fig. 5. (a–j): Plots of decay of coda-normalized peak amplitudes for P- and S-waves with hypocentral distances at six central frequencies for DDI (Dehradun) station. The dotted line shows the best fitted line using the least-squares method.

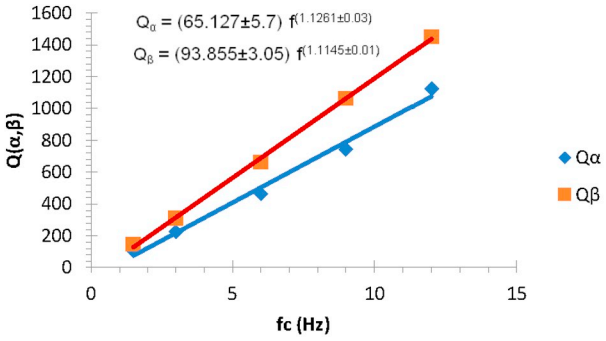

(a)

(b)

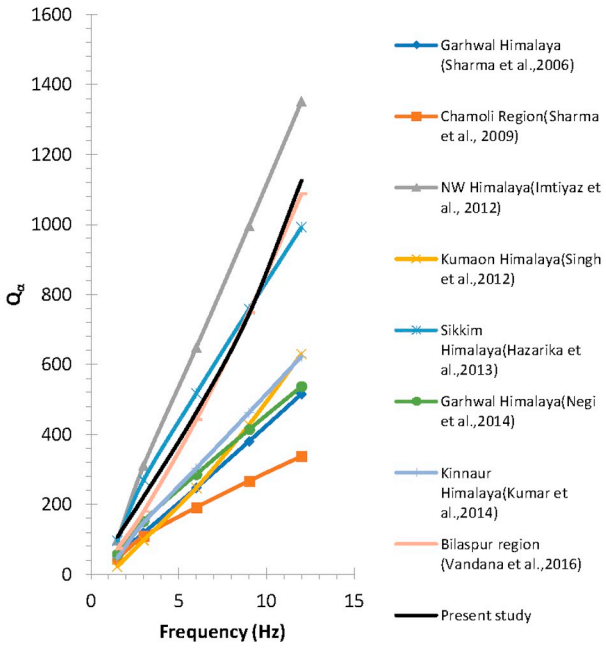

(c)

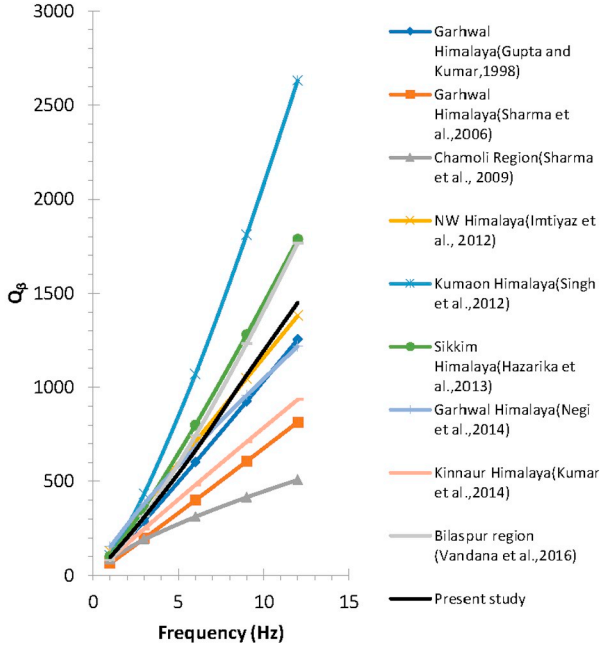

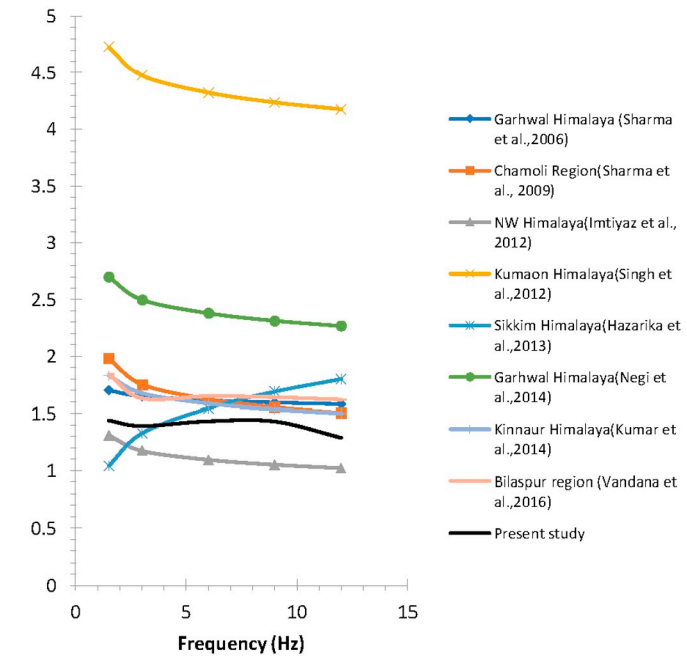

(d)

(caption on next page)

Fig. 6. (a) Comparison between average Q_α and Q_β; (b) Comparison of estimate, Q_α with other parts of the Himalayan region; (c) Same as that of (b) but for Q_β; (d) Comparison of Q_β/Q_α values with the other Himalayan regions.

have distinctly different sensitivity to shear waves. Comparison of the average Q_β/Q_α vs frequency (Fig. 6d), which shows a systematic variation in pattern of Q_β/Q_α which is found to be similar in almost all Himalaya belts, except in the Sikkim Himalaya region (Eastern Himalayan) estimated by Hazarika et al. (2013) that suggested a conspicuous variation in attenuation for the Himalayan region at varying frequency.

The present study is almost comparable with the Garhwal Himalaya (Sharma et al., 2006), Chamoli region of Garhwal Himalaya (Sharma et al., 2009), the Kinnaur and Bilaspur regions of the Himachal Himalaya (Kumar et al., 2014; Vandana et al., 2016) because it shows similar attenuation characteristics in all the regions of the Himalayas. Based on the Q_β/Q_α estimates obtained by various investigators, it has been concluded that NW Himalayan and its surrounding region has the average Q_β/Q_α estimates that varies from 1.29 to 1.44 in the frequency range from 1 to 12 Hz. In the present study, we obtained $Q_\alpha \leq Q_\beta$, which indicates that the presence of partially saturated rocks in NW Himalaya region correspond to rocks with fractures and cracks associated with air and fluids through the process of imbibition (replacing air from cracks and fractures by fluids) that might have made the cracked and fractured rocks partially saturated and attributed to lowering of P-wave velocity whilst S-wave velocity became higher due to high sensitivity of S-wave towards the fluids even due to partial saturation that causes high Q_β. In presence of fluids in the rock matrix and extent of saturation using 3-D velocity tomography for different regions demonstrated how the sensitivity of S-wave towards fluids influences the degree of structural heterogeneity (Zhao et al., 2002; Mishra and Zhao, 2003; Mishra et al., 2003; Mukhopadhyay et al., 2006; Mishra et al., 2008; Lei et al., 2009; Singh et al., 2012; Mishra, 2013; Lei et al., 2019, Lei and Zhao, 2016; Zhou and Lei, 2016) that is why Q_β is found to be higher in the study region. Our results are also in good corroboration with the earlier studies (Vassiliou et al., 1982) based on laboratory experiments for sedimentary rocks, which showed relationship between Q_α and Q_β as: $Q_\alpha \leq Q_\beta$ for partially saturated rocks and $Q_\alpha > Q_\beta$ for fully saturated rocks (Vassiliou et al., 1982). Fig. 7a shows seismological coupling coefficient represented by average variation in kappa (κ) values for different tectonic Zones, suggesting the Zone between Lesser Himalaya (LH) and Higher Himalaya (HH) [Zone-III] with the highest coupling coefficient corresponds to the least attenuative property of coda (Q_c^{-1}), P-wave (Q_α^{-1}) and S-wave (Q_β^{-1}) associated with higher value of quality factor (Q_c, Q_α, Q_β) is Zone of higher strength in comparison to the other two Zones between Sub Himalaya (SH) and Lesser Himalaya (LH) [Zone-II] and the Zone between Indo-Gangetic-Plain (IGP) and the Sub Himalaya (SH) [Zone-I], which in turn suggests that seismic strength for Zone-III has capability to generate seismic moment of higher magnitude earthquakes (Fig. 7b; Table 4) with less seismic attenuation that may generate strong seismic energy to cause comparatively higher earthquake hazards. It is further observed that Zone-I between IGP and SH is partitioned by Himalayan Frontal Thrust (HFT) and is associated with several geological known faults, namely Vaikrita thrust, Ropar Fault, Moradabad fault in addition to encroachment of Munsiari Thrust and Delhi-Haridwar Ridge that may have attributed to the relatively high seismic attenuation in Zone-I and Zone-II. It is interesting to note that seismic activity of different Zones is different (Table 4) because of varying attenuative property of Zones associated with several exposed and hidden seismogenic faults, causing variation in the structural heterogeneity. Role of structural heterogeneity estimated in terms of seismic velocity, source and path characteristics has already been documented by other researchers for other regions (Sharma and Wason, 1994; Zhao et al., 2002; Mishra et al., 2008; Mishra, 2014; Tripathi et al., 2014; Vandana et al., 2017; Vandana and Mishra, 2019; Ekka et al., 2019), which supports our interpretation of attenuation characteristics of the media and their interrelationship with structural heterogeneity.

4.1. Seismotectonic implications

Under the Himalayan arc there are different dip angles of the subducting Indian slab from the west to the east. In the east, the dip angle is much steeper (Li et al., 2008; Lei et al., 2009; Lei et al., 2019; Lei and Zhao, 2016; Zhou and Lei, 2016) in comparison to that of in the west where the dip of the subducting Indian plate is reported to be much smaller (Li et al., 2008; Zhou and Lei, 2016; He et al., 2018). In the present study, we mainly focus on the attenuation structure (Q_c; Q_α; Q_β) in the west segment of the Hiamalyan arc. It has been observed that the average attenuation values for different geo-tectonic blocks demarcated as Zone-I to Zone-III (Fig. 8a–b) have conspicuous and distinct variations in estimates of average seismic attenuation characteristics (Q_c; Q_α; Q_β) that were made for respective blocks. It is observed that average coda wave quality factor (Q_c), average quality factor for P-wave (Q_α), and S-wave (Q_β) in the Higher Himalaya (HH) has the highest estimates in comparison to those of the Indo Gangetic Plain (IGP), the Sub Himalaya (SH), and the Lesser Himalaya (LH). Conversely, the attenuative property of all three tectonic Zones bears relationship in terms of its variability of Q_c^{-1}, Q_α^{-1} and Q_β^{-1} as: $Q_c^{-1}(LH) > Q_c^{-1}(SH) > Q_c^{-1}(IGP) > Q_c^{-1}(HH)$; $Q_\alpha^{-1}(LH) > Q_\alpha^{-1}(SH) > Q_\alpha^{-1}(IGP) > Q_\alpha^{-1}(HH)$; and $Q_\beta^{-1}(LH) > Q_\beta^{-1}(SH) > Q_\beta^{-1}$ (IGP) $> Q_\beta^{-1}$ (HH) as shown in Table 3(c). We interpreted that average attenuation values at Lesser Himalaya is more attenuative to the Sub Himalaya (SH), the Indo Gangetic Plain (IGP) and the Higher Himalaya (HH). We found that the lesser Himalayas located south of the Greater Crystalline Himalayan sequence and bounded by MCT in the north and MBT in the south. The region mainly consists of Proterozoic and lower Paleozoic sedimentary rocks. These rocks are metamorphosed to greenschist facies. The region also consists of Paleocene-Eocene limestone, shale (the Subathu formation), synclinal (klippen) and anticlines outliers of Greater Himalayan metamorphic rocks, which may have contributed to the highest degree of attenuation in the Lesser Himalaya (Fig. 8a–b). The MCT is a longitudinal thrust fault, act as a main separator between the higher Himalaya and the lesser Himalaya. It is worth to notice that the MCT is a contact between the terrigenous carbonate rocks and thick overlying metamorphic rocks, gneiss and mica schists (Sinha, 1987) that could have attributed to different attenuative behaviour of the Higher and the Lesser Himalaya. The retrograde metamorphic series is also found in the fault system that consisted of crystalline rocks at the top of Higher Himalayan Zone to Paleozoic sediments in the form of klippen in synclines in the lesser Himalayan Zone. It is, therefore the tectonic Zones associated with the Lesser Himalaya and the Higher Himalaya have different attenuative property. On the other hand, the Sub-Himalaya (Himalayan foreland) Zone consists of clastic sediments, which were formed during the uplift and erosion of the Himalaya and deposited by rivers in a foreland basin. The molasse of Sub-Himalayan is faulted and folded to form low altitude mountain ranges known as Siwalik Hills and the Sub-Himalaya has overthrusted by lesser Himalaya along MBT that significantly contributed to the higher attenuation value in Zone-II (Fig. 8a–b). The MBT is a steep thrust, which gets flattened with depth, whilst the Sub-Himalaya is bounded by the Himalayan Frontal thrust (HFT) to the south and overthrusted along the Holocene alluvial tracts of the Indo-Gangetic plains along the Main Frontal Thrust (MFT) or the Himalayan Frontal Thrust (HFT) (Ni and Barazangi, 1984) that may have made Zone-I moderate to high attenuative Zones in comparison to those of Sub Himalaya and the Lesser Himalaya. On the other hand, the Indo Gangetic Plain is found less attenuative in comparison to those of SH and the LH because the Indo - Gangetic Plain is surrounded by Delhi Haridwar Ridge and Moradabad fault, which are transversal in the foothills, showing traces of neotectonics and recent activity (Arur and Hasija, 1986). It is observed that because of the development of the E-W trending tensional stress in this thrust environment and high concentration of earthquake epicentres, the Delhi-Haridwar Ridge (DHR) is considered as one of the vulnerable areas for earthquake hazards of NW Himalaya (Valdiya, 1976). The strike-slip faulting in the Uttarkashi region is also supposed to be due to the extension of the DHR (Khattri, 1992, 1998). On the other hand, this region is very less attenuative at Higher Himalaya because Higher Himalaya Crystalline (HHC) formations with a 30-km-thick remained as medium - to high-grade metamorphic sequence of meta-sedimentary rocks that are intruded in many places by granites of Ordovician age (c. 500 Ma) and early Miocene (c. 22 Ma) age. It is pertinent to mention that along the Satluj River, the Higher Himalayan Crystalline rocks shows an inverted metamorphic field characterized by garnet-staurolite rocks at the base, kyanite and sillimanite in the middle and migmatite Barrovian mineral units at the bottom (Vannay and Grasemann, 1998), besides the HH block is also associated with Mica schist, quartzite, paragneiss, migmatite, and leucogranite bodies with the multiphase deformation even at low pressure conditions

Table 2
P-wave quality factor (Q_α) and S-wave quality factor (Q_β) values along with their Standard errors (σ) and number of events (N) at different central frequencies at 13-stations.

Central frequency (fc)	Station name/Station code (Ayanagar/AYAN) $Q_\alpha \pm \sigma$ $Q_\beta \pm \sigma$		N	Station name/Station code (Bahadurgarh/BHGR) $Q_\alpha \pm \sigma$ $Q_\beta \pm \sigma$		N	Station name/Station code (Bisrakh/BIS) $Q_\alpha \pm$ $Q_\beta \pm \sigma$		N	Station name/Station code (Dehradun/DDI) $Q_\alpha \pm \sigma$ $Q_\beta \pm \sigma$		N
1.50	89.04 ± 0.002	97.46 ± 0.003	80	80.29 ± 0.01	104.63 ± 0.001	191	81.07 ± 0.002	88.38 ± 0.002	174	72.61 ± 0.001	95.99 ± 0.001	79
3.00	149.46 ± 0.002	203.28 ± 0.002	80	183.54 ± 0.001	212.38 ± 0.001	191	143.98 ± 0.002	175.67 ± 0.002	174	170.43 ± 0.001	222.69 ± 0.001	79
6.00	296.27 ± 0.003	415.46 ± 0.003	80	402.46 ± 0.002	517.44 ± 0.001	191	327.43 ± 0.001	382.00 ± 0.002	174	388.42 ± 0.001	388.42 ± 0.001	79
9.00	523.10 ± 0.001	683.02 ± 0.002	80	569.39 ± 0.001	694.12 ± 0.001	191	459.69 ± 0.002	646.80 ± 0.002	174	705.72 ± 0.002	618.59 ± 0.002	79
12.00	697.47 ± 0.001	940.80 ± 0.002	80	759.19 ± 0.001	925.50 ± 0.001	191	636.27 ± 0.002	925.50 ± 0.002	174	982.47 ± 0.002	902.82 ± 0.001	79
Average	Q0 = 52.561 ± 3.93	Q0 = 60.321 ± 2.85		Q0 = 54.61 ± 4.14	Q0 = 67.33 ± 10.2		Q0 = 52.03 ± 9.4	Q0 = 53.932 ± 7.65		Q0 = 47.78 ± 17.1	Q0 = 63.84 ± 5.3	
	ɵ = 1.033 ± 0.03	ɵ = 1.108 ± 0.02		ɵ = 1.072 ± 0.02	ɵ = 1.08 ± 0.06		ɵ = 0.999 ± 0.94	ɵ = 1.119 ± 0.04		ɵ = 1.169 ± 0.09	ɵ = 1.055 ± 0.03	

Central frequency (fc)	Station name/Station code (Dhramshala/DHRM) $Q_\alpha \pm \sigma$ $Q_\beta \pm \sigma$		N	Station name/Station code (Joshimath/JOSI) $Q_\alpha \pm \sigma$ $Q_\beta \pm \sigma$		N	Station name/Station code (Kalagarh/KALG) $Q_\alpha \pm \sigma$ $Q_\beta \pm \sigma$		N	Station name/Station code (Khetri/KHE) $Q_\alpha \pm \sigma$ $Q_\beta \pm \sigma$		N
1.50	126.53 ± 0.002	245.88 ± 0.001	373	103.09 ± 0.001	129.36 ± 0.001	286	154.64 ± 0.001	138.15 ± 0.001	183	149.12 ± 0.001	290.40 ± 0.001	167
3.00	287.96 ± 0.003	570.45 ± 0.001	373	245.61 ± 0.002	287.46 ± 0.001	286	222.69 ± 0.002	279.01 ± 0.001	183	327.49 ± 0.001	444.67 ± 0.001	167
6.00	879.05 ± 0.004	1462.70 ± 0.001	373	457.59 ± 0.004	618.67 ± 0.001	286	422.83 ± 0.001	542.08 ± 0.001	183	451.40 ± 0.001	918.03 ± 0.001	167
9.00	1318.58 ± 0.005	2444.79 ± 0.001	373	603.69 ± 0.002	880.18 ± 0.001	286	726.18 ± 0.002	992.76 ± 0.001	183	659.29 ± 0.001	1355.20 ± 0.001	167
12.00	2226.95 ± 0.003	3457.29 ± 0.002	373	824.79 ± 0.003	1237.35 ± 0.001	286	997.14 ± 0.001	1478.40 ± 0.001	183	867.64 ± 0.001	1674.07 ± 0.001	167
Average	Q0 = 61.95 ± 7.6	Q0 = 143.56 ± 4.92		Q0 = 78.63 ± 9.4	Q0 = 83.98 ± 8.58		Q0 = 79.213 ± 5.87	Q0 = 89.907 ± 7.86		Q0 = 110.13 ± 17.1	Q0 = 186.7 ± 12.9	
	ɵ = 1.466 ± 0.05	ɵ = 1.285 ± 0.01		ɵ = 0.938 ± 0.03	ɵ = 1.09 ± 0.04		ɵ = 0.938 ± 0.03	ɵ = 1.162 ± 0.03		ɵ = 0.847 ± 0.08	ɵ = 0.891 ± 0.02	

Central frequency (fc)	Station name/Station code (Kurukshetra/KKR) $Q_\alpha \pm \sigma$ $Q_\beta \pm \sigma$		N	Station name/Station code (Kundal/KUDL) $Q_\alpha \pm \sigma$ $Q_\beta \pm \sigma$		N	Station name/Station code (Rohtak/RTK) $Q_\alpha \pm \sigma$ $Q_\beta \pm \sigma$		N	Station name/Station code (Shimla/SMLA) $Q_\alpha \pm \sigma$ $Q_\beta \pm \sigma$		N
1.50	65.24 ± 0.001	94.86 ± 0.001	164	198.83 ± 0.002	233.27 ± 0.001	181	99.41 ± 0.002	114.75 ± 0.002	182	94.89 ± 0.001	225.86 ± 0.001	356
3.00	154.64 ± 0.001	215.60 ± 0.001	164	439.52 ± 0.001	558.02 ± 0.001	181	222.69 ± 0.002	212.38 ± 0.003	182	245.61 ± 0.001	527.02 ± 0.001	356
6.00	280.70 ± 0.001	418.51 ± 0.001	164	927.89 ± 0.001	1323.68 ± 0.001	181	538.77 ± 0.002	580.80 ± 0.002	182	491.23 ± 0.001	918.03 ± 0.001	356
9.00	451.40 ± 0.001	723.53 ± 0.001	164	1616.33 ± 0.001	2371.60 ± 0.001	181	945.40 ± 0.001	797.92 ± 0.002	182	863.90 ± 0.001	1355.20 ± 0.001	356
12.00	575.93 ± 0.001	1034.88 ± 0.002	164	3036.75 ± 0.001	2845.92 ± 0.001	181	1484.63 ± 0.001	1116.04 ± 0.002	182	1363.43 ± 0.001	1997.13 ± 0.001	356
Average	Q0 = 46.513 ± 4.5	Q0 = 61.69 ± 12.5		Q0 = 107.87 ± 23.9	Q0 = 139.03 ± 29.9		Q0 = 56.266 ± 7.76	Q0 = 69.465 ± 7.7		Q0 = 44.28 ± 5.6	Q0 = 52.55 ± 8.43	
	ɵ = 1.011 ± 0.03	ɵ = 1.105 ± 0.06		ɵ = 1.288 ± 0.10	ɵ = 1.263 ± 0.10		ɵ = 1.2902 ± 0.04	ɵ = 1.123 ± 0.04		ɵ = 0.842 ± 0.11	ɵ = 0.86 ± 0.05	

Central frequency (fc)	Station name/Station code (Sona/SONA) $Q_\alpha \pm \sigma$ $Q_\beta \pm \sigma$		N
1.50	88.84 ± 0.002	128.19 ± 0.002	123
3.00	231.97 ± 0.001	276.30 ± 0.001	123
6.00	451.40 ± 0.001	558.02 ± 0.001	123
9.00	705.72 ± 0.001	959.29 ± 0.001	123
12.00	927.89 ± 0.001	1279.06 ± 0.001	123
Average	Q0 = 63.001 ± 4.45	Q0 = 80.948 ± 4.8	
	ɵ = 1.0861 ± 0.02	ɵ = 1.1098 ± 0.02	

Table 3
(a–c): Variation in Q_c, Q_α and Q_β in and around various geo-tectonic units as demarcated in Fig. 1.

(a)Average attenuation relationships for coda waves (Q_c), P-waves (Q_α) and S-waves (Q_β)

Geotectonic segments of NW Himalaya	Seismological indicators		
	$Q_c = (Q_0 \pm \sigma)f^n$	$Q_\alpha = (Q_0 \pm \sigma)f^n$	$Q_\beta = (Q_0 \pm \sigma)f^n$
Indo Gangetic Plain (IGP)	$Qc = (147 \pm 30)f^{(1.06\pm0.04)}$	$Q_\alpha = (128 \pm 11.2)f^{(0.84\pm0.03)}$	$Q_\beta = (170 \pm 28.1)f^{(1.15\pm0.05)}$
Sub Himalaya (SH)	$Qc = (107 \pm 11)f^{(1.19\pm0.03)}$	$Q_\alpha = (94 \pm 11.5)f^{(1.11\pm0.06)}$	$Q_\beta = (142 \pm 43.2)f^{(0.89\pm0.11)}$
Lesser Himalaya (LH)	$Qc = (106 \pm 9)f^{(1.17\pm0.04)}$	$Q_\alpha = (84 \pm 12.8)f^{(1.06\pm0.04)}$	$Q_\beta = (105 \pm 9.5)f^{(1.14\pm0.04)}$
Higher Himalaya (HH)	$Qc = (156 \pm 17.9)f^{(1.00\pm0.04)}$	$Q_\alpha = (149 \pm 19.4)f^{(1.09\pm0.03)}$	$Q_\beta = (196 \pm 20.4)f^{(0.84\pm0.05)}$

(b) Average quality values at frequencies varying between 1.5 and 12 Hz

Geotectonic segments of NW Himalaya	Seismological indicators		
	$(Q_{c\ (MIN.)}, Q_{c\ (MAX.)})$	$(Q_{\alpha\ (MIN.)}, Q_{\alpha\ (MAX)})$	$(Q_{\beta\ (MIN.)}, Q_{\beta\ (MAX)})$
Indo Gangetic Plain (IGP)	(196, 2698)	(214, 1565)	(296, 2995)
Sub Himalaya (SH)	(153, 3036)	(163, 2569)	(169, 1962)
Lesser Himalaya (LH)	(142, 2786)	(117, 1789)	(161, 3049)
Higher Himalaya (HH)	(252, 2561)	(225, 3340)	(323, 2668)

(c) Average attenuation values at different frequencies (1.5 to 12 Hz)

Geotectonic segments of NW Himalaya	Seismological indicators		
	$(Q_{c(MIN.)}^{-1}, Q_{c(MAX.)}^{-1})$	$(Q_{\alpha\ (MIN.)}^{-1}, Q_{\alpha\ (MAX.)}^{-1})$	$(Q_{\beta\ (MIN.)}^{-1}, Q_{\beta\ (MAX.)}^{-1})$
Indo Gangetic Plain (IGP)	(0.0051, 0.00037)	(0.0046, 0.00063)	(0.0033, 0.00033)
Sub Himalaya (SH)	(0.0065, 0.00032)	(0.0061, 0.00038)	(0.0059, 0.00051)
Lesser Himalaya (LH)	(0.0070, 0.00035)	(0.0085, 0.00055)	(0.0062, 0.00032)
Higher Himalaya (HH)	(0.0039, 0.00039)	(0.0044, 0.00029)	(0.0030, 0.00037)

(Sorkhabi and Macfarlane, 1999), which supports our inference of the least attenuation in the Higher Himalayan Zone-III (Fig. 7b). Our interpretation of distinct variation in Q structure of the Higher Himalaya Crystalline (HHC) belt is found to be in unison with the earlier studies based on surface wave attenuation and source characterization of the Tibet region (Singh and Gupta, 1979; Singh and Gupta, 1982). Therefore, oblique oriented faults across or oblique to the Himalayan longitudinal strike used to experience recent activity. The earthquake activity is both the thrust and the strike-slip faulting where these transverse faults cross the Himalayan thrust belt. Perhaps, the Quaternary activity at some places in the MCT Zone is also associated with the strike-slip movement along the transverse faults.

Our results demonstrated that degree of structural heterogeneities associated with different types of seimogenic faults, mineralogical compositions, and intricate tectonic settings bear strong correlation with sesimogenesis in NW Himalaya and its surrounding region. The seismic potential of generating higher magnitude earthquakes ($M > 4.0$) is principally associated with Zone-III in comparison to those of Zone-II and Zone-I, which suggests that earthquake of moderate to strong magnitude for a given depth of occurrence have plausible correspondence to Zone-III, which may cause relatively more earthquake hazards due to its least attenuative charcaterstics (Fig. 8a–b; Table 4). This is also supported by high kappa (κ) value in the Higher Himalaya Zone and is found to be in unison to the earlier study made on source characterization of NW Himalaya region by Vandana and Mishra (2019), which is supportive to the Steady State model of Seeber et al. (1981), which argues for great Himalayan earthquakes related to the detachment surface where MCT and MBT converge and forms the interface between the subducting Indian Plate (Li et al., 2008; Mishra, 2014; Lei and Zhao, 2016; Lei et al., 2019,) and overlying sedimentary wedge. The seismicity in the tectonic Zones demarcated as Zone-I to Zone-II found to be very much correlative to the varying estimates of attenuative characteristics and number of earthquakes ($M > 4.0$), which shows a close correspondence as $M_o(HH) > M_o(LH) > M_o(IGP) > M_o(SH)$ (Fig. 7b; Table 4) with varying numbers (N) of earthquakes ($(M > 4.0)$ $N(HH) > N(LH) > N(IGP) > (SH)$ (Fig. 7c and Table 4). This observation is in good unison to the evolutionary model (Ni and Barazangi, 1984) that enunciates that the MBT is the most active tectonic feature and seismicity is concentrated to 50 km wide Zone between surface trace of MBT and the MCT [Fig. 7(b–c); Fig. 8(a–b); Table 4].

5. Summary

In the present study we estimated the frequency-dependent attenuation characteristics of P-waves (Q_α), S-waves (Q_β) and coda waves (Q_c) using 515 micro to moderate earthquakes ($2.5 \le M \le 5.0$) recorded between January 2008 and November 2015 for a central frequency range (f_c) varying from 1.5 to 12 Hz for the north-west (NW) Himalaya and its surrounding region. We obtained average attenuation relationships of Q_c, Q_α and Q_β as: $Q_c = (126.94 \pm 37.9).\ f^{(1.122\pm0.06)}$, $Q_\alpha = (65.127 \pm 5.7).f^{(1.1261\pm0.03)}$ and $Q_\beta = (93.855 \pm 3.05).f^{(1.1145\pm0.01)}$ for NW Himalaya and its surrounding region. We obtained $Q_\alpha \le Q_\beta$, which indicates the presence of partially saturated rocks in north-west Himalaya region that may correspond to rocks with fractures and cracks associated with fluids through the process of imbibitions (replacing air from cracks and fractures by fluids) that might have made the cracked and fractured rocks partially saturated and attributed to lowering of P-wave velocity whilst S-wave velocity became higher due to high sensitivity of S-wave towards the fluids even due to partial saturation that might have attributed to high-Q_β. It is found that the nature and extent of seismic attenuation are different for different seismotectonic belts consisted of various kinds of fault systems distributed into the Indo Gangetic Plain (IGP), the Sub Himalaya (SH), the Lesser Himalaya (LH), and the Higher Himalaya (HH) beneath NW Himalaya and its surrounding region. It is also observed that material property heterogeneity beneath the subsurface earth is playing an important role in influencing the degree of release of seismic energy in NW Himalaya and its surrounding region because of varying attenuative property in different geotectonic segments as:

$$Q^{-1}\alpha,\ \beta,\ c(HH) < Q^{-1}\alpha,\ \beta,\ c(IGP) < Q^{-1}\alpha,\ \beta,\ c(SH) < Q^{-1}\alpha,\ \beta,\ c(LH)$$

It has been demonstrated that degree of structural heterogeneities associated with different types of seimogenic faults, different mineralogical compositions of rocks, and intricate tectonic settings bear strong correlation with

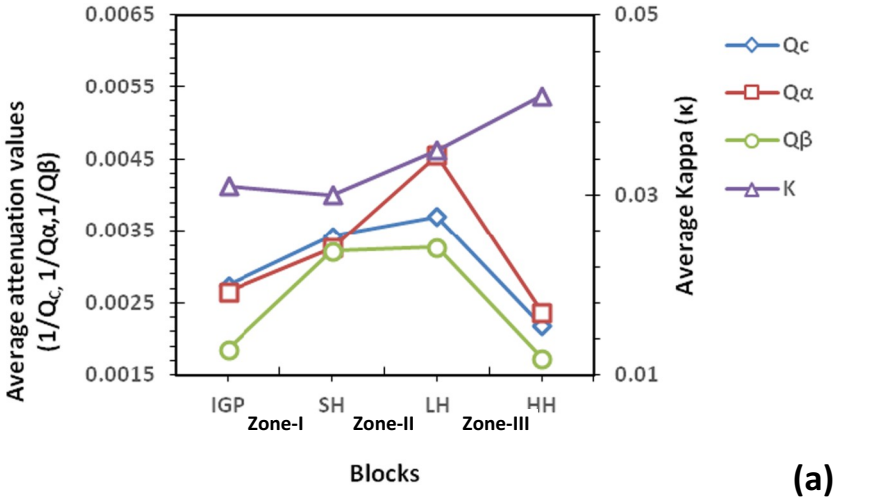

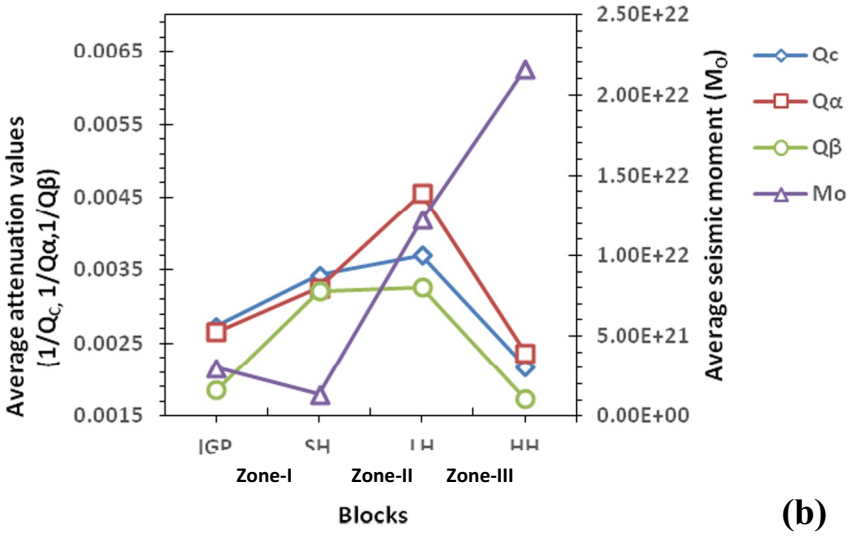

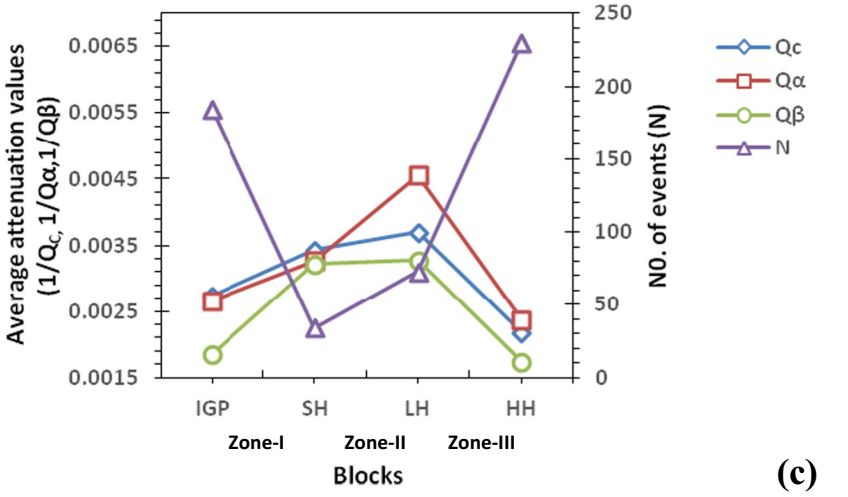

Fig. 7. (a) Plot of average attenuation values in different tectonic blocks of NW Himalaya region with respect to average kappa (κ) values; (b) Plot between average attenuation values in different tectonic blocks of NW Himalaya region with average seismic moment estimated from earthquakes used in this study; (c) Plot between average attenuation values in different blocks of NW Himalaya region and the number of events (N) used in this study.

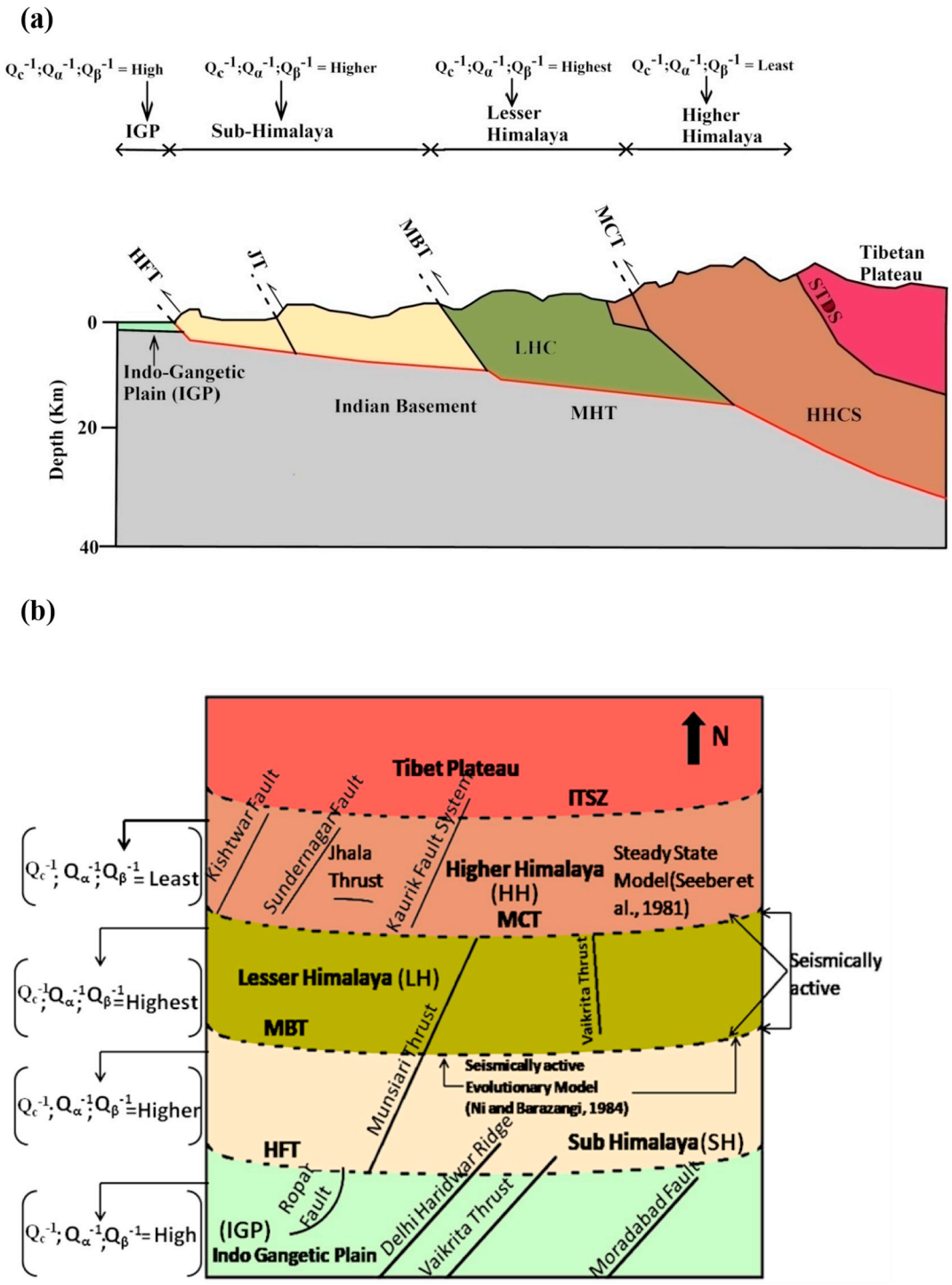

Fig. 8. (a) Cross section of the NW Himalayan region [modified from Day, 2016]; (b) A schematic model deduced from this study showing the distribution of seismic attenuation strength in NW Himalayan region; IGP: Indo - Gangetic Plain; SH: Sub-Himalaya; LH: Lesser Himalaya; HH: Higher Himalaya; LHC: Lesser Himalayan Crystalline; HHCS: High Himalayan Crystalline Series: STDS: South Tibet Detachment System; ITSZ: Indo – Tsangpo Suture Zone.

Table 4
Distribution of attenuation parameters (Q_c; Q_α; Q_β), kappa (κ) and seismic moment (M_o) along with the distribution of number (N) of earthquakes (M > 4.0) used in this study for different tectonic blocks.

Tectonic blocks	Q_c^{-1}	Q_α^{-1}	Q_β^{-1}	Kappa (κ)	Seismic moment (Mo) (dyne cm)[a]	No. of events (N)	M > 4.0
IGP (below HFT)	0.002736	0.002656	0.001856	0.031	3.02E + 21	184	2
SH (between HFT and MBT)	0.003433	0.003262	0.003213	0.030	1.36E + 21	34	1
LH (between MBT and MCT)	0.003701	0.004553	0.00327	0.039	1.22E + 22	73	5
HH (above MCT)	0.002179	0.002372	0.001735	0.041	2.16E + 22	230	27

[a] Earthquake catalogue (2008–2015) used in this study.

sesimogenesis in NW Himalaya and its surrounding region. The seismic potential of generating higher magnitude earthquakes (M > 4.0) is principally associated with Zone-III in comparison to those of Zone-II and Zone-I, which suggests that earthquake of moderate to strong magnitude for given depth of occurrence have propensity to Zone-III, which may cause relatively more earthquake hazards due to its least attenuative characteristics. This observation is also supported by comparatively higher kappa (κ) value in the Higher Himalaya Zone, which supports the Steady State model, which argues for great Himalayan earthquakes related to the detachment surface where MCT and MBT converge and forms the interface between the subducting Indian Plate and overlying sedimentary wedge. The seismicity in the tectonic Zones demarcated as Zone-I to Zone-II found to be very much correlative to the varying estimates of attenuative characteristics and number of earthquakes (M > 4.0), which shows a close correspondence to the variation of seismic moment as: M_o (HH) > M_o(LH) > M_o(IGP) > M_o(SH) with varying numbers (N) of earthquakes ((M > 4.0) as N(HH) > N(LH) > N(IGP) > N(SH). This observation is in accordance to the evolutionary model, enunciating that the MBT is the most active tectonic feature and seismicity is concentrated to 50 km wide Zone between surface trace of MBT and the MCT. Our proposed schematic model for NW Himalaya and its surrounding region shed an important light in detail on attenuation characteristics of different tectonic blocks associated with both local and regional fault system that dictates the source characteristics and potential of earthquake hazards of NW Himalaya region of analogous tectonic settings, elsewhere in the world.

CRediT authorship contribution statement

O.P. Mishra: Writing - original draft, Writing - review & editing, Formal analysis, Investigation. **Vandana:** Investigation, Data curation, Formal analysis. **Vikas Kumar:** Data curation, Visualization. **Sasi Kiran Gera:** Data analysis and data compilation.

Declaration of competing interest

The authors declare that they have no known competing financial interests or personal relationships that could have appeared to influence the work reported in this paper.

Acknowledgements

The authors are thankful to the Secretary, Ministry of Earth Sciences (MoES), Government of India for support and encouragement to conduct this piece of research using the own in-house seismological data recorded by seismological network ascribed to National Centre for Seismology (NCS), MoES, New Delhi. Authors express thanks to the Director, NCS, MoES, New Delhi for providing congenial academic environment for carrying out this study at the Centre. The authors also acknowledge continued support of all colleagues of NCS-MoES during analysis of data. We prepared some of figures using the Generic Mapping Tool (GMT) package (Wessel and Smith, 1991). Authors are thankful to three anonymous reviewers for their critical and constructive reviews and to Vernon Cormier, Editor, PEPI for is comments that improved the original manuscript significantly.

References

Aki, K., 1969. Analysis of seismic coda of local earthquakes as scattered waves. J. Geophys. Res. 74, 615–631.
Aki, K., 1980. Attenuation of shear waves in the lithosphere for frequencies from 0.05 to 25 Hz. Phys. Earth Planet. Interiors 21, 50–60.
Aki, K., Chouet, B., 1975. Origin of coda waves: source, attenuation and scattering effects. J. Geophys. Res. 80, 3322–3342.
Akinci, A., Taktak, A.G., Ergintav, S., 1994. Attenuation of coda waves in Western Anatolia. Phys, Earth Planet. Interiors 87, 155–165 Arita.
Arita, K., 1983. Origin of inverted metamorphism of the lower Himalaya, Central Nepal. Tectonophysics 95, 43–60.
Arur, M.G., Hasija, N.L., 1986. Crustal movement studies across Ganga Tear Fault (in Shivaliks) at Haridwar in U.P. India. In: Proceedings of the International Symposium on Neotectonics in South Asia, Dehradun, India. 330. pp. 44.
Atkinson, G.M., Mereu, R.F., 1992. The shape of ground motion attenuation curves in Southeastern Canada. Bull. Seismol. Soc. Am. 82, 2014–2031.
Barros, L.V., Assumpcao, M., Quintero, R., Ferreira, V.M., 2011. Coda wave attenuation in the Parecis Basin Amazon craton – Brazil–sensitivity to basement depth. J. Seismol. 15, 391–409.
Bath, M., 1974. Introduction to Seismology. Wiley & Sons, New York.
Boatwright, J., 1978. Detail spectral analysis of two small New York State earthquakes. Bull. Seism. Soc. Am. 68, 1117–1131.
Boatwright, J., Fletcher, J.B., Fumal, T.E., 1991. A general inversion scheme for source, site, and propagation characteristics using multiply recorded sets of moderate-sized earthquakes. Bull. Seism. Soc. Am. 81, 1754–1782.
Boulanouar, A., El Moudnib, L., Harnafi, M., Cherkaoui, T.E., Rahmouni, A., Boukalouch, M., Sebbani, J., 2013. Spatial variation of coda wave attenuation using aftershocks of the Al Hoceima earthquake of 24 February, 2004. Morocco. Nat. Sci. 5 (08), 72.
Burg, J.P., Leyreloup, A., Girardeau, J., Chen, G.M., 1987. Structure and metamorphism of a tectonically thickened continental crust—the Yalu Tsangpo suture Zone (Tibet). Philos. Trans. R. Soc. Lond. Ser. A 321, 67–86.
Canas, J.A., Pujades, L., Badal, J., Payo, G., de Miguel, F., Alguacil, G., Ibanez, J., Morales, J., 1991. Lateral variation and frequency dependence of coda–Q in the Southern part of Iberia. Geophys. J. Inter. 107, 57–66.
Chopra, S., Kumar, D., Rastogi, B.K., 2010. Attenuation of high frequency P and S waves in the Gujarat Region, India. Pure Appl. Geophys. 168, 797–813.
Das, R., Mukhopadhyay, S., Singh, R.K., Baidya, P.R., 2018. Lapse time and frequency-dependent coda wave attenuation for Delhi and its surrounding regions. Tectonophysics 738–739, 51–63.
Dobrynina Anna, A., 2011. Coda-wave attenuation in the Baikal rift system lithosphere. Phys. Earth and Planet. Interiors 188, 121–126.
Ekka, M.S., Vandana, Roy, P.N.S. and Mishra, O.P., 2019. Coda wave seismic structure beneath the Indian Ocean region and its implications to seismotectonics and structural heterogeneity. J. Asian Earth Sci. https://doi.org/10.1016/j.jeaes.2019.104104.
Fehler, M., Roberts, P., Fairbanks, T., 1988. A temporal change in coda wave attenuation observed during an eruption of Mount St. Helens. J. Geophys. Res. 93, 4367–4373.
Fletcher, J.B., 1995. Source parameters and crustal Q for four earthquakes in South Carolina. Seism. Res. Lett. 66, 44–58.
Frankel, A., McGarr, A., Bicknell, J., Mori, J., Seeber, L., Cranswick, E., 1990. Attenuation of high frequency shear waves in the crust: measurements from New York State, South Africa and Southern California. J. Geophys. Res. 96, 6269–6289.
Gansser, A., 1964. Geology of the Himalayas. Interscience, London 289.
Gao, L.S., Biswas, N.N., Lee, L.C., Aki, K., 1983. Effects of multiple scattering on coda waves in three dimensional medium. Pure Appl. Geophys. 121, 3–15.
Gholamzadeh, A., Rahimi, H., Yaminifard, F., 2013. Spatial and temporal variation of coda-wave attenuation in the Faryab region, southeast of the Sanandaj–Sirjan zone, using aftershocks of the Tiab earthquake of 28 February 2006. Bull. Seismol. Soc. Am. 104 (1), 529–539.
Gupta, S.C., Teotia, S.S., Rai, S.S., Gautam, N., 1998. Coda Q estimates in the Koyna region, India. Pure Appl Geophys 153, 713–731.
Havskov, J., Malone, S., Mcclurg, D., Crosson, R., 1989. Coda Q for the state of Washington. Bull. Seism. Soc. Am. 79, 1024–1038.
Hazarika, P., Kumar, M.R., Kumar, D., 2013. Attenuation character of seismic waves in Sikkim Himalaya. Geophys. J. Int. 195, 544–557.
He, P., Lei, J., Yuan, X., Xu, X., Xu, Q., Liu, Z., Mi, Q., Zhou, L., 2018. Lateral Moho variations and the geometry of the Main Himalayan Thrust beneath the Nepal Himalayan orogeny revealed by teleseismic receiver functions. Geophys. J. Int. 214, 1004–1017.
Hellweg, M., Spandich, P., Fletcher, J.B., Baker, L.M., 1995. Stability of coda-Q in the region of Parkfield, California: view from the U.S. Geological Survey Parkfield Dense Seismograph Array. J. Geophys. Res. 100, 2089–2102.
Herrmann, R.B., Kijko, A., 1983. Modelling some empirical vertical component Lg relations. Bull. Seism. Soc. Am. 73, 157–171.
Hoshiba, M., 1993. Separation of scattering attenuation and intrinsic absorption in Japan using the Multiple Lapse Time Window Analysis of full seismogram envelope. J. Geophys. Res. 98, 15809–15824.
Hough, S.E., 1997. Empirical Green's function analysis: taking the next step. J. Geophys. Res. 102, 5369–5384.
Hough, S., Anderson, J.G., Brune, J., Vernon, F., Berger, J., Fletcher, J., Haar, L., Hanks, T., Baker, L., 1988. Attenuation near Anza, California. Bull. Seism. Soc. Am. 78, 672–691.
Ibanez, J.M., Delpezzo, E., Demiguel, F., Herraiz, M., Alguaicil, G., Morales, J., 1990. Depth dependent seismic attenuation in the Granada Zone (Southern Spain). Bull. Seism. Soc. Am. 80, 1232–1244.
Imtiyaz, A.P., Preeti, Y., Nagaraj, K., 2012. Attenuation of P, S and Coda waves in the NW-Himalayas, India. International Journal of Geosciences 3, 179–191.
Jin, A., Aki, K., 1988. Spatial and temporal correlation between coda Q and seismicity in China. Bull. Seismol. Soc. Am. 78, 741–769.
Khattri, K.N., 1992. Local seismic investigations in the Garhwal-Kumaun Himalaya. In: Gupta, G.D. (Ed.), Himalayan seismicity. India, Geol. Soc., pp. 45–66.
Khattri, K.N., 1998. Local seismic investigations in the Garhwal-Kumaon Himalaya. Memoir Geol. Soc. India 23, 45–66.
Khattri, K.N., Chander, R., Gaur, V.K., Sarkar, I., Kumar, S., 1989. New seismological results on the tectonics of the Garhwal Himalaya, proceedings of the Indian Academy of Sciences (*Earth and Planetary sciences)*. Bull. Seism. Soc. Am. 98 (1), 91–109.
Kumar, N., Parvez, I.A., Virk, H.S., 2005. Estimation of Coda Waves Attenuation for NW Himalayan Region Using Local Earthquakes. Research Report CM 0404, C MMACS, India.
Kumar, N., Mate, S., Mukhopadhyay, S., 2014. Estimation of Q_α and Q_β of Kinnaur Himalaya. Journal of Seism. 18, 47–59.
Kumar, Vikas, Kumar, Dinesh, Chopra, Sumer, 2016. Estimation of source parameters and scaling relations for moderate size earthquakes in North-West Himalaya. J. Asian Earth Sci. 128. https://doi.org/10.1016/j.jseaes.2016.07.023.
Kumar, V., Kumar, D., Chopra, S., 2019. Source Parameters and Scaling Relations for Moderate Size Earthquakes in North–East India Region. Pure Appl. Geophys. 176, 45–64. https://doi.org/10.1007/s00024-018-1972-0.
Latchman, J.L., Ambeh, W.B., Lynch, L.L., 1996. Attenuation of seismic waves in the Trinnidad and Tobago area. Tectonophysics 253, 111–127.
Lei, J., Zhao, D., 2016. Teleseismic P-wave tomography and mantle dynamics beneath eastern Tibet. Geochem. Geophys. Geosyst. 17, 1861–1884.
Lei, J., Zhao, D., Su, Y., 2009. Insight into the origin of the Tengchong intraplate volcano and seismotectonics in southwest China from local and teleseismic data. J. Geophys. Res. 114,

B05302. https://doi.org/10.1029/2008JB005881.
Lei, J., Xie, F., Mishra, O.P., Zhang, G., Lu, Y., Li, Y., 2012. The 2011 Yingjiang, China, earthquake (M 5.8): a volcano-related fluid-driven earthquake? Bull. Seismol. Soc. Am. 102, 417–425.
Lei, J., Zhao, D., Xu, X., Xu, Y., Du, M., 2019. Is there a big mantle wedge under eastern Tibet? Phys. Earth Planet. Inter. 292, 100–113.
Li, B.J., Qin, J.Z., Qian, X.D., Ye, J.Q., 2004. The coda attenuation of the Yaoan area in Yunnan Province. Acta Seismol. Sin. 17 (1), 47–53.
Li, C., van der Hilst, R., Meltzer, A., Engdahl, E., 2008. Subduction of the Indian lithosphere beneath the Tibetan Plateau and Burma. Earth Planet. Sci. Lett. 274, 157–168.
Mahood, M., Hamzehloo, H., 2009. Estimation of coda wave attenuation in East Central Iran. J. Seismol. 13, 125–139.
Mak, S., Chan, L.S., Chandler, A.M., Koo, R.C.H., 2004. Coda Q estimates in the Hong Kong Region. J. Asian Earth Sci. 24, 127–136.
Mishra, O.P., 2012. Seismological research in India (2007–2011). Proceeds. Ind. Nat. Sci. Acad. Publication (PINSA) 76 (3), 361–375.
Mishra, O.P., 2013. Crustal Heterogeneity in Bulk Velocity beneath the 2001 Bhuj earthquake source zone and its implications. Bull. Seismol. Soc. Am. 103 (6), 3235. https://doi.org/10.1785/0120110144.
Mishra, O.P., 2014. Intricacies of Himalayan seismotectonics and seismogenesis: need of an integrated research. Curr. Sci. 106 (2), 176–187.
Mishra, O.P., Zhao, D., 2003. Crack density, saturation rate and porosity at the 2001 Bhuj, India, earthquake hypocenter: a fluid-driven earthquake? Earth Planet. Sci. Lett. 212, 393–405.
Mishra, O.P., Zhao, D., Umino, N., Hasegawa, A., 2003. Tomography of northeast Japan forearc and its implications for interplate seismic coupling. Geophys. Res. Lett. 30. https://doi.org/10.1029/2003GL017736.
Mishra, O.P., Zhao, D., Wang, Z., 2008. The genesis of the 2001 Bhuj, India, earthquake (Mw 7.6): a puzzle for Peninsular India. J. Indian Minerals Special Issue 61 (3–4), 149–170 & 62 (1–4).
Mishra, O.P., Zhao, D., Ghosh, C., Wang, Z., Singh, O.P., Ghosh, B., Mukherjee, K.K., Saha, D.K., Chakrabortty, G.K., Gaonkar, S.G., 2011. Role of crustal heterogeneity beneath Andaman–Nicobar Islands and its implications for coastal hazard. Nat. Hazards 57, 51–64.
Mishra, O.P., Singh, A.P., Kumar, D., Rastogi, B.K, 2014. An insight into Crack density, Saturation rate and Porosity model of the 2001 Bhuj earthquake in the Stable Continental Region of Western India. J. Asian Earth Sci. 83, 48–59.
Mohamed, H.H., Deif, A., Ibrahim, H.A., Abuel-enean, K., El-Amin, E.M., 2010. Source parameters of the 2007 earthquake sequence, Aswan, Egypt. Journal of African Earth Sciences 62, 19–25.
Mukhopadhyay, S., Mishra, O.P., Zhao, D., Kayal, J.R., 2006. 3-D seismic structure of the source area of the 1993 Latur, India, earthquake and its implications for rupture nucleations. Tectonophysics 415, 1–16.
Mukhopadhyay, S., Tyagi, C., 2007. Lapse time and frequency-dependent attenuation characteristics of coda waves in the Northwestern Himalayas. J. Seismol. 11 (2), 149–158.
Nakata, T., 1989. Active faults of the Himalaya of India and Nepal. Geol. Soc. Am. Pap. 232, 243–264.
Negi, S.S., Paul, A., Joshi, A., and Kamal (2014), Body wave crustal attenuation characteristics in the Garhwal Himalaya, India, Pure Appl. Geophys. doi:https://doi.org/10.1007/s00024-014-0966-9.
Ni, J., Barazangi, M., 1984. Seismotectonics of the Himalayan collision zone: geometry of the underthrusting Indian plate beneath the Himalaya. J. Geophys. Res. 89, 1132–1146.
Parvez, I.A., Sutar, A.K., Mridula, M., Mishra, S.K., Rai, S.S., 2008. Coda Q estimates in the Andaman Islands using local earthquakes. Pure Appl. Geophys. 165, 1861–1878.
Paul, A., Gupta, S.C., Pant, C.C., 2003. Coda Q estimates for Kumaon Himalaya. Proc Ind Acad Sci (Earth Planet Sci) 112, 569–576.
Pujades, L., Canas, J.A., Egozcue, J.J., Puigvi, M.A., Pous, J., Gallart, J., Lana, X., Casas, A., 1991. Coda Q distribution in Iberian Peninsula. Geophys. J. Int. 100, 285–301.
Pulli, J.J., 1984. Attenuation in New England. Bull. Seismol. Soc. Am. 74, 1149–1166.
Rahimi, H., Hamzehloo, H., 2008. Lapse time and frequency-dependent attenuation of coda waves in the Zagros continental collision Zone in Southwestern Iran. J. Geophys. Eng. 5, 173–185.
Rai, S.S., Priestley, I.K., Gaur, V.K., Mitra, S., Singh, M.P., Searle, M., 2006. Configuration of the Indian Moho beneath NW Himalaya and Ladakh. Geophys. Res. Lett. 33.
Rautian, T.G., Khalturin, V.I., 1978. The use of the coda for the determination of the earthquake source spectrum. Bull. Seism. Soc. Am. 68, 923–948.
Roecker, S.W., Tucker, B., King, J., Hartzfield, D., 1982. Estimates of Q in Central Asia as a function of frequency and depth using the coda of locally recorded earthquakes. Bull. Seism. Soc. Am. 72, 129–149.
Rovelli, A., 1982a. On the frequency dependence of Q in Friuli from short period digital records. Bull. Seism. Soc. Am. 72, 2369–2372.
Rovelli, A., 1982b. On the frequency dependence of Q in Friuli from short period digital records. Bull. Seism. Soc. Am. 72, 2369–2372.
Sato, H., 1977. Energy propagation including scattering effects: single isotropic approximation. J. Phys. Earth 25, 27–41.
Scherbaum, F., Kisslinger, C., 1985. Coda Q in the Adak seismic zone. Bull. Seismol. Soc. Am. 75, 615–620.
Seeber, L., Armbruster, J.G., Quitt-Meyer, R.C., 1981. Seismicity and continental subduction in the Himalayan arc. In: Zagros, Hindu-Kush, Himalaya, Geodynamic Evolution, Geodyn. Am. Geophys. Union. 3. pp. 215–242.
Sharma, M.L., Wason, H.R., 1994. Occurrence of low stress drop earthquakes in the Garhwal Himalaya region. Phys. Earth Planet. Inter. 85 (3–4), 265–272.
Sharma, B., Teotia, S.S., Kumar, D., 2006. Frequency Dependent Attenuation of High Frequency P and S Waves in the Upper Crust of Garhwal, Himalaya, 6th International Conference & Exposition on Petroleum Geophysics, Kolkata.
Sharma, B., Teotia, S.S., Kumar, D., 2007. Attenuation of P, S and coda waves in Koyna region India. J. Seismol. 11, 327–344.
Sharma, B., Gupta, A.K., Devi, D.K., Kumar, D., Teotia, S.S., Rastogi, B.K., 2008. Attenuation of high-frequency seismic waves in Kachchh Region, Gujarat, India. Bull. Seismol. Soc. Am. 98, 2325–2340.
Sharma, B., Teotia, S.S., Kumar, D., Raju, P.S., 2009. Attenuation of P and S waves in the Chamoli Region, Himalaya, India. Pure Appl. Geophys. 166 (12), 1949–1966.
Singh, D.D., Gupta, H.K., 1979. Source mechanism and surface wave attenuation studies for Tibet earthquakes of July 14, 1973. Bull. Seism. Soc. Am. 69, 737–750.
Singh, D.D., Gupta, H.K., 1982. Q-Structure beneath the Tibetan Plateau from the inversion of Love-and Rayleigh waves attenuation data. Phys. Earth and Planet. 29, 183–194.
Singh, C., Singh, A., Bharathi, V.K.S., Bansal, A.R., Chadha, R.K., 2012. Frequency-dependent body wave attenuation characteristics in the Kumaun Himalaya. Tectonophysics 524–525, 37–42.
Sinha, A.K., 1987. Tectonic Zonation of the Central Himalayas and the crustal evolution of collision and compressional belts. Tectonophysics 134, 59–74.
Sorkhabi, Rasoul B., and Macfarlane, A. (1999) Himalaya and Tibet: mountain roots to mountain tops, in Macfarlane, A., Sorkhabi, R.B, and Quade, J., eds., Himalaya and Tibet: Mountain Roots to Mountain Tops, Geol. Survey of America Special Paper vol. 328, 1–8.
Tripathi, J.N., Singh, P., Sharma, M.L., 2014. Attenuation of high-frequency P and S waves in Garhwal Himalaya, India. Tectoniphysics 636, 216–227.
Valdiya, K.S., 1976. Himalaya transverse faults and fold and their parallelism with subsurface structures of North Indian planes. Tectonophysics 32, 353–386.
Valdiya, K.S., 1979. An outline of the structural set-up of the Kumaon Himalaya. J. Geol. Soc. India 20, 145–157.
Valdiya, K.S., 1987. Trans-Himadri Thrust and domalupwarps immediately south of collision zone and tectonic implications. Curr. Sci. 56, 200–209.
Valdiya, K.S., 1989. Trans-Himadri intra crustal fault and basement upwarps south of the Indus-Tsangpo Suture Zone. Geol. Soc. Amer. Spec. 153–168.
Valdiya, K.S., 1998. Dynamic Himalaya. 178 Univ. Press, Hyderabad, India.
Vandana, Kumar, A., Gupta, S.C., 2016. Attenuation characteristics of body-waves for the Bilaspur Region of Himachal Lesser Himalaya. Pure and Appl Geophys 173, 447–462.
Vandana, Mishra, O.P., 2019. Source characteristics of the NW Himalaya and its adjoining region: geodynamical implications. Phys. Earth Planet. Inter. 294, 106277. https://doi.org/10.1016/j.pepi.2019.106277.
Vandana, Gupta, S.C., Kumar, A., 2015. Coda wave attenuation characteristics for the Bilaspur region of Himachal Lesser Himalaya. Nat. Hazards 78, 1091–1110.
Vandana, Kumar, Ashwani, Gupta, S.C., Mishra, O.P., Kumara, Arun, Sandeep, 2017. Source parameters and high frequency characteristics of local events ($0.5 \leq M_L \leq 2.9$) around Bilaspur region of the Himachal Himalaya. Pure and Appl. Geophysics 174, 1643–1658.
Vannay, J.-C., Grasemann, B., 1998. Inverted metamorphism in the High Himalaya of Himachal Pradesh (NW India): phase equilibriaversus thermobarometry. Schweiz. Mineral. Petrogr. Mitt. 78, 107–132.
Vargas, C.A., Ugalde, A., Pujades, L.G., Canas, J.A., 2004. Spatial variation of coda wave attenuation in northwestern Columbia. Geophys. J. Int. 158, 609–624.
Vassiliou, M., Salvado, C.A., Tittman, B.R., 1982. Seismic attenuation. In: Carmichael, R.S. (Ed.), CRC Handbook of Physical Properties of Rocks. 3 CRC Press, Boca Raton, Florida.
Wessel, P., Smith, W.H.F., 1991. Free software helps map and display data. EOS Trans. AGU 72, 441.
Woodgold, C., 1994. Coda-Q in Charlevoix, Quebec, Region. Lapse time dependence and spatial and temporal comparisons. Bull. Seismol. Soc. Am. 84, 1123–1131.
Wu, R.S., 1985. Multiple scattering and energy transfer of seismic waves-seperation of scattering effect from intrinsic attenuation-I. Theoretical modeling. Geophys. J.R. Astr. Soc. 82, 57–80.
Yin, A., Harrison, T.M., 2000. Geologic evolution of the Himalayan-Tibetan orogen. Annu. Rev. Earth Planet. Sci. 28, 211–280.
Yoshimoto, K., Sato, H., Ohtake, M., 1993. Frequency-dependent attenuation of P and S waves in the Kanto area, Japan, based on the coda normalization method. Geophys. J. Int. 114, 165–174.
Zhao, D., Mishra, O.P., Sanda, R., 2002. Influence of fluid and magma on earthquakes: seismological evidence. Phys. Earth Planet. Inter. 132, 249–267.
Zhao, D., Tani, H., Mishra, O.P., 2004. Crustal heterogeneity in the 2000 western Tottori earthquake region: effect of fluids from slab dehydration. Phys. Earth Planet. Inter. 145, 161–177.
Zhou, Z., Lei, J., 2016. Pn anisotropic tomography and mantle dynamics beneath China. Phys. Earth Planet. Inter. 257, 193–204.